Running Head: Cholinergic Control of Transcription and Pathology

Cholinergic surveillance over hippocampal RNA metabolism and Alzheimer's-like pathology

Benjamin Kolisnyk[1,2,+], Mohammed Al-Onaizi[1,4,+], Lilach Soreq[5], Shahar Barbash[6], Uriya Bekenstein[6], Nejc Haberman[5], Geula Hanin[6], Maxine T. Kish[1,3], Jussemara Souza da Silva[1], Margaret Fahnestock[7], Jernej Ule[5], Hermona Soreq[6], Vania F. Prado[1,2,3,4,8,*], Marco A. M. Prado[1,2,3,4,8,*]

1 Robarts Research Institute, 2 Graduate Program in Neuroscience, 3 Department of Physiology and Pharmacology, 4 Department of Anatomy & Cell Biology, Schulich School of Medicine & Dentistry, University of Western Ontario, London, Ontario, Canada, N6A5K8

5 Department of Molecular Neuroscience, UCL Institute of Neurology, Queen Square, London WC1N 3BG, UK

6 The Edmond and Lily Safra Center for Brain Science and The Silberman Institute of Life Sciences, The Edmond J Safra Campus, The Hebrew University of Jerusalem, Israel, 91904

7 Department of Psychiatry and Behavioural Neurosciences, McMaster University, Hamilton, ON, Canada L8S 4K1

Footnotes [+]Co-First authors, [8]Co-Senior authors

*To whom correspondence should be addressed:

Marco Prado mprado@robarts.ca, Vania Prado vprado@robarts.ca

Robarts Research Institute, University of Western Ontario, 1151 Richmond St London, Ontario, Canada, N6A 5K8

Keywords: Acetylcholine, Alzheimer's Disease, Cognition, Pathology, RNA Metabolism

Abstract

The relationship between long-term cholinergic dysfunction and risk of developing dementia is poorly understood. Here we used mice with deletion of the vesicular acetylcholine transporter (VAChT) in the forebrain to model cholinergic abnormalities observed in dementia. Whole genome RNA-sequencing of hippocampal samples revealed that cholinergic failure causes changes in RNA metabolism. Remarkably, key transcripts related to Alzheimer's disease are affected. *BACE1* for instance, shows abnormal splicing caused by decreased expression of the splicing regulator hnRNPA2/B1. Resulting BACE1 overexpression leads to increased APP processing and accumulation of soluble $A\beta_{1-42}$. This is accompanied by age-related increases in GSK3 activation, tau hyper-phosphorylation, caspase-3 activation, decreased synaptic markers, increased neuronal death and deteriorating cognition. Pharmacological inhibition of GSK3 hyperactivation reversed deficits in synaptic markers and tau hyperphosphorylation induced by cholinergic dysfunction, indicating a key role for GSK3 in some of these pathological changes. Interestingly, in human brains there was a high correlation between decreased levels of VAChT and hnRNPA2/B1 levels with increased tau hyperphosphorylation. These results suggest that changes in RNA processing caused by cholinergic loss can facilitate Alzheimer's-like pathology in mice, providing a mechanism by which decreased cholinergic tone may increase risk of dementia.

Introduction

Alzheimer's disease (AD), the predominant form of dementia, is pathologically characterized by accumulation of amyloid plaques and neurofibrillary tangles that ultimately lead to neuronal death. One of the early alterations identified in AD-affected individuals with cognitive decline is a profound decrease in basal forebrain cholinergic neurons (Whitehouse et al., 1982), which gave rise to the cholinergic hypothesis of AD (Bartus et al., 1982). Accordingly, Alzheimer's Disease Neuroimaging Initiative data reveal atrophy of the basal forebrain in individuals with mild cognitive impairment (Grothe et al., 2014), and increased forebrain cholinergic atrophy in Alzheimer's-affected individuals (Grothe et al., 2013). Cholinergic dysfunction correlates with decreased hippocampal volume and pathology (Teipel et al., 2014). Furthermore, recent epidemiological data suggest that long-term use of drugs with anti-cholinergic activity by elderly individuals increases the future risk of dementia (Gray et al., 2015). These observations reveal an intimate, but poorly understood relationship, between cholinergic dysfunction and the pathological and cognitive deficits in AD. However, whether cholinergic malfunction has a causal role in increasing the risk of dementia or regulating pathology is unknown. Moreover, the causal and temporal relationships between cholinergic malfunctioning and long-term changes in hippocampal neurons in AD are still unclear.

To test the capacity of cholinergic tone to regulate long-term functions in target cells we examined the hippocampal transcriptome in genetically-modified mice with compromised hippocampal cholinergic tone. Using forebrain-specific deletion of the vesicular acetylcholine transporter (VAChT), a protein required for acetylcholine (ACh) release (de Castro et al., 2009; Prado et al., 2013), we unveil that long-term cholinergic deficiency causes global changes in gene expression and alternative splicing in the hippocampus. This leads to abnormal alternative splicing of BACE1 with consequent age-dependent changes in amyloid precursor protein (APP) processing, tau hyper-phosphorylation, hippocampal neuronal loss and cognitive decline. Comparative analyses in the AD brain enabled us to identify links between cholinergic deficiency and AD pathology, together supporting the notion that early cholinergic dysfunction may be a pivotal step in AD pathology initiation and progression. Our data provide potential mechanisms to explain how cholinergic deficiency may facilitate pathology in AD.

Materials and Methods

Mouse lines

Generation of VAChT$^{flox/flox}$ mice was previously described (de Castro et al., 2009). VAChT$^{Nkx2.1\text{-}Cre\text{-}flox/flox}$ mice were generated by crossing VAChT$^{flox/flox}$ (crossed for 5 generations with C57BL/6J) with the Nkx2.1-Cre mouse line (C57BL/6J-Tg(Nkx2-1-cre)2Sand/J), purchased from The Jackson Laboratory (JAX stock no. 008661). Unless otherwise stated, all control mice used were VAChT$^{flox/flox}$ littermates. All procedures were conducted in accordance with guidelines of the Canadian Council of Animal Care (CCAC) and in accordance with ARRIVE guidelines, at the University of Western

Ontario with an approved institutional animal protocol (2008-127). Only male mice were used for all experiments.

RNA Sequencing

Mouse hippocampal tissue was rapidly dissected and total RNA was extracted from individual samples using the PureLink RNA Mini Kit (Ambion). 2 µg of total RNA were then sent to the Centre for Applied Genomics, The Hospital for Sick Children, where the cDNA library was prepared using the TruSeq Stranded Total Sample Preparation kit (Illumina) and run in a HiSeq 2500 platform with coverage of 200-250 million pair reads per lane. 5 animals were run per lane to obtain enough coverage for alternative splicing analysis (50 million pair reads per sample). The sequenced reads were aligned to the mouse genome using the TopHat program against the mouse genome in Ensembl (version EnsMart72) to enable quantification of splice junctions in addition to gene level measurements. Differential gene expression analysis was conducted using the Bioconductor DESeq package which accounts for the counts binomial distribution (Anders and Huber, 2010). Datasets are available on ArrayExpress (http://www.ebi.ac.uk/arrayexpress/) under accession number E-MTAB-3897.

For human brains, we used the SQUARE^{TM} RNA library construction approach which utilizes different sets of 5'- and 3'-site specific primers to segregate all full-length transcripts into sub-pools defined by the selective nucleotides in the respective primers. Unlike traditional sequencing, which is based on the use of universal primers that produce a pool of fragmented RNA products for a given gene, we used 12 different sets of 3'-primers that complement all distinct di-nucleotides at transcript 3'-polyadenylation sites and enable separate sequencing of the corresponding intact RNA molecules for

each of the primer sets through barcoding. This unprecedented depth of segregated brain RNA-Seq data was made publicly accessible by establishing a user-friendly website where the sequenced variants for any given brain-expressed transcript can be found (http://apainad.weebly.com/). Sequencing files were processed and analyzed for differential expression and functional enrichment.

RNA sequencing libraries made from the temporal gyrus samples yielded an average of $6.0*10^6$ ($STD=2.0*10^6$) uniquely aligned 75 base pair (bp) single end reads, or approximately $7.0*10^7$ ($STD=1.8*10^7$) total read counts when combining all 12 SQUARE fields for each sample. These reads were mapped against the GRGCh37/hg19 version of the *Homo sapiens* genome (http://genome.ucsc.edu/). Transcripts with more than 1 read per kilobase per million (RPKM) per SQUARE field were defined as being detected (Hebenstreit and Teichmann, 2011). An average of 6610±1367 genes per field were detected across the 12 fields (details in Supplementary Table III). Expression criteria were set to RPKM>1 in at least one of the SQUARE fields, in at least 80% of the tested donor cohorts.

Immunofluorescence

Immunofluorescence experiments were performed as previously described (de Castro et al. 2009). Primary antibodies used were anti-Choline Transporter (CHT1; 1:200), which was kindly donated by Dr. R. Jane Rylett, University of Western Ontario, London, Ontario, anti-hnRNPA2/B1 (1:200 Santa Cruz Biotechnology Catalog no. sc-10035), anti-Cleaved caspase-3 (1:500 Thermo Fisher Scientific, Catalog no. PA5-16335), anti-AT180 (1:1000 Thermo Fisher Scientific, Catalog no. EN-MN1040), anti-NeuN (1:200 PhoshphoSolutions, Catalog no. 583-FOX3), anti-GFAP, anti-PSD95.

Sections were visualized by Zeiss LSM 510 Meta (Carl Zeiss, Oberkochen, Germany) confocal system (40x, 63x objectives, with an N.A. of 1.3 and 1.4, respectively) and by Leica TCS SP8 (Leica Microsystems Inc, Ontario, Canada) confocal system (63x objective, with an N.A. of 1.4), a 488-nm Ar laser and 633-nm HeNe laser were used for excitation of fluorophores.

Western Blotting

Mouse hippocampi were collected, protein was isolated, and immunoblotting was performed as previously described using RIPA lysis buffer supplemented with protease and phosphatase inhibitors (Guzman et al., 2011). Band intensities were quantified using FluoroChemQ software (Thermo Fisher Scientific).

Gene Ontology Analysis

Gene ontology functional analysis was performed using the GOrilla software through the web application. Using the two-un-ranked lists method as described (Eden et al., 2009). KEGG pathway analysis was performed using the ClueGO plug-in of Cytoscape (Bindea et al., 2009).

RNA Binding Protein Analysis

To predict potential RNA-binding proteins that may be implicated in the observed changes in alternative splicing, alternatively spliced sequences were run through the RBPmap software (Paz et al., 2014) to detect potentially altered RNA binding proteins. The list of RNA binding proteins that were suggested by the software were then run through the Allen Brain Atlas (http://mouse.brain-map.org/) in order to ensure that they

were expressed in the murine hippocampus. All RNA binding proteins not expressed in the hippocampus were excluded.

qPCR

To measure mRNA expression, total RNA was extracted from freshly dissected hippocampal tissue, using the Aurum Total RNA for fatty and fibrous tissue kit (Bio-Rad) according to the manufacturer's instructions. cDNA synthesis and qPCR analysis were performed as previously described (Guzman et al., 2011). For alternative splicing experiments, the alternative exon levels were normalized to a constitutively expressed exon from the same gene.

Primary Neuronal Cultures

Primary mouse hippocampal neurons were produced from E16 embryos as previously described (Ostapchenko et al., 2013). Neurons were cultured for 15 days. Knockdown of hnRNPA2/B1 from the cultured neurons was achieved by treatment with a shRNA, as previously described (Berson et al., 2012). A separate set of cultured neurons was treated with 10μM of carbachol, 10μM of carbachol and 100μM Atropine, or 100μM Atropine alone for 48 hours.

APP Processing

Biochemical analysis of the processing of APP was performed as previously described (Dewachter et al., 2002). Forebrains from VAChT deficient and control mice were homogenized in 50mM Tris-HCl (pH 8.5), samples were then ultracentrifuge at 135,000g for 1 hour at 4^{o}C, and the supernatant was collected and analyzed by

Western blotting and ELISA. The pellet was re-suspended and ultracentrifuged again and diluted in 8M guanidine HCl to obtain the insoluble fraction for ELISA analysis.

ELISA

Murine β-amyloid was measured from the hippocampal homogenate using the Wako Human/Rat (Mouse) β-Amyloid (42) ELISA High-Sensitive Kit (Catalog Number: 292-64501). The ELISA assay was performed according to the manufacturer's protocol.

Congo Red Staining

Congo red staining was performed as previously described (Thompson and Walker, 2015), using a Congo-Red solution (Sigma C-6277) in 100% ethanol.

Silver staining

Assessment of argyrophilic cells in the hippocampus was done by using NeuroSilverTM staining kit II (FD NeuroTechnologies, Inc., Baltimore, MD), which provides detection of degenerating neurons, including neuronal somata, axons, and terminals.

Estimation of Hippocampal Volume

NeuN immunohistochemistry was performed in order to estimate the volume of and number of neurons of hippocampal regions CA1, CA3, and the dentate gyrus (DG) as described (Beauquis et al., 2014). Briefly, tissue sections were stained with mouse monoclonal anti-NeuN (1:500 PhosphoSolutions, Catalog no. 583-FOX3), using the ABC kit (Vector Laboratories) and developed with 2 mM diaminobenzidine (Sigma, USA) and 0.5 mMH_2O_2 in 0.1 M Tris buffer. The total number of NeuN (*T*) cells in the

various hippocampal regions was estimated using the following formula: $T = \frac{N*V}{t}$, where N is the cell density, V is the volume of the structure, and t is the thickness of the section.

GSK3 Inhibition

To inhibit GSK3 in VAChT$^{Nkx2.1\text{-}Cre\text{-}flox/flox}$ mice, a cohort of aged animals (12 months old, n=5 AR-A014418 treated, n=4 saline treated) were implanted with Alzet micro-osmotic pumps (Model 1004; DURECT Corp, Cupertino, Calif). The pumps were implanted subcutaneously in the intra-scapular region of each mouse. The reservoir of each pump was preloaded with 96 µL of either sterile saline solution or the GSK3 inhibitor AR-A014418. The pumps administered 5 mg/kg/d of AR-A014418, a dose shown to produce a significant inhibition of GSK3 *in vivo* (Ly et al., 2013). During the implantation procedure, mice were anesthetized with ketamine (100 mg/kg) and xylazine (15 mg/kg). Drug treatment lasted for 28 days.

Morris Water Maze

The spatial version of the Morris water maze (MWM) was conducted as described previously to investigate spatial memory (Kolisnyk et al., 2013b; Martyn et al., 2012; Vorhees and Williams, 2006). Briefly, animals were given four training trials a day (90 s each) for 4 d, with a 15 minute inter-trial interval. If the mice did not find the platform after 90 s during the learning phase, they were gently directed to the platform. On the fifth day, memory was assessed via a probe trial (60 s), during which the platform is removed and time spent in the target quadrant is measured. The task was performed in a 1.5-m-diameter pool with 25°C water. The platform was submerged 1 cm

below the surface of the water, and spatial cues (posters, streamers, and plastic props) were distributed around the pool. Sessions were recorded and analyzed using the ANY-Maze Software.

The classification of search strategies mice employed during training was defined as previously described (Garthe et al., 2009). An experimenter blind to genotypes scored search strategies as follows: (1) thigmotaxis, characterized by maintaining close proximity to the wall (>70% trial within 10-cm of wall); (2) random search, illustrated by global swimming with no classified strategy; (3) scanning, characterized by a preference for the central pool area (>50% trial within 35-cm of pool center); (4) chaining, characterized by searching near the correct radial distance of the platform to the wall (>75% trial 20–50-cm from the pool center, <15% within 10-cm of wall, and <10% within 20-cm of pool center); (5) directed search, characterized by a preference for a passageway toward the platform or platform quadrant (>80% trial within a 50-cm-wide region from the start point to the platform); (6) focal search, characterized by a highly localized search near the platform (≥50% trial in a circular target zone with a 15-cm radius); (7) direct swim, characterized by a maintained heading toward the platform (Little to no deviation in path to reach platform from start point). Total block lengths were the sum of all blocks for one strategy and one mouse.

Protein Isolation from Human post-mortem brain tissue.

Samples from parietal cortical tissues from age/ sex-matched controls (n = 6, 3 females and 3 males) and AD-affected individuals (n = 6, 3 females and 3 males) and information related to age and demographics have been previously published (Ostapchenko et al., 2013). The samples were homogenized in RIPA buffer

supplemented with protease inhibitor cocktail (Calbiochem), and Western blotting was performed as described above.

Statistical analysis

Sigmastat 3.5 software was used for statistical analysis. Student's t-test was used for comparison between two experimental groups. Two-way ANOVA or two-way ANOVA with repeated measures (RM) were used when more than two groups were compared.

Results

Forebrain Cholinergic dysfunction modifies expression levels of hippocampal transcripts and alternative splicing

To determine the contribution of cholinergic tone to the regulation of hippocampal transcript levels, we used VAChT$^{Nkx2.1\text{-}Cre\text{-}flox/flox}$ mice, a mouse line with selective deletion of the VAChT gene from forebrain regions, including the medial septum, which contains cholinergic neurons that project to the hippocampus. VAChT has been shown to be essential for ACh packaging and release (de Castro et al., 2009; Lima Rde et al., 2010; Prado et al., 2006). Non-biased whole genome transcriptome RNA-sequencing of hippocampal samples from three VAChT-deficient and four control mice yielded a total of 14,200 expressed genes. Comparative analysis revealed that 1,098 genes were differentially expressed in VAChT$^{Nkx2.1\text{-}Cre\text{-}flox/flox}$ hippocampi compared to control mice (Figure 1A-B, FDR corrected $p < 0.05$). Of those, 763 genes were upregulated and 362 down-regulated in the transgenic mice. In addition, a linear regression analysis on reciprocal junction pairs detected roughly 4% of hippocampal transcripts in VAChT$^{Nkx2.1\text{-}}$

$^{Cre\text{-}flox/flox}$ mice as alternatively spliced in high confidence as compared with control mice. Equal proportion of exon inclusion and exclusion events was observed; mainly events of cassette exons were detected (Figure 1C), suggesting widespread changes in several splicing regulation related pathways and/or cellular mechanisms (Soreq et al., 2014).

We interrogated these differentially expressed/spliced genes for involvement in neuronal function and AD-like pathology. A number of genes involved in critical pathways including PI3K-Akt signalling pathway [a regulator of neuronal vulnerability (Endo et al., 2006; Gary and Mattson, 2001)], spliceosome regulation and regulation of microtubule-based processes were identified using Gene Ontology (GO) KEGG pathway analysis (Figure 1D, Table SI). qPCR validation and correlation between changes observed in RNA-Seq and in an independent mouse cohort are shown in Figure S1 for the different gene pathways and alternative splicing events. These results suggest that abnormal cholinergic signalling can effectively modulate several major gene pathways with potential to influence the function of target cells in the hippocampus.

We also performed small molecule RNA-Seq and additional miRNA microarray hybridization experiments, and observed limited changes in miRNA expression in the hippocampus of VAChT-deficient mice (Figure S2). VAChT$^{Nkx2.1\text{-}Cre\text{-}flox/flox}$ hippocampus showed a mature miRNA expression profile with only marginal differences from controls. Only 7 of 700 detectable miRNAs were differentially expressed, and of the 20 miRNAs most highly expressed in the hippocampus, comprising 82% of total counts, none were differentially expressed (Figure S2). These findings point to alternative

splicing and transcription, or changes in mRNA turnover, rather than miRNA, as potential main contributors to phenotypes in VAChT-deficient mice.

Cholinergic deficit triggers abnormal BACE1 alternative splicing and APP Processing

One of the detected abnormally alternatively spliced genes in our database was the protease BACE1 (Figure 1D), which is responsible for the cleavage of APP (Luo et al., 2001). The predicted alternative splicing event in VAChT-deficient mice is expected to increase expression of BACE1-501, the active protein isoform (Mowrer and Wolfe, 2008). qPCR analysis validated the predicted splicing event and demonstrated increased exon 3/4 inclusion for *BACE1* (Figure 2A).

Bioinformatics analysis using the *RBP-Map* tool revealed an enrichment of binding sites for hnRNPA2/B1 in *BACE1* mRNA. hnRNPA2/B1 is part of a family of RNA binding proteins that regulate pre-mRNA splicing, trafficking and maturation (Bekenstein and Soreq, 2013). Notably, AD-associated impairments in cholinergic signalling are accompanied by decreased expression of hnRNPA2/B1 protein in the AD cerebral cortex and in cholinergic impaired mice (Berson et al., 2012; Kolisnyk et al., 2013a). Correspondingly, the hippocampus of VAChT$^{Nkx2.1\text{-}Cre\text{-}flox/flox}$ mice showed reduced hnRNPA2/B1 protein levels (Figure 2B). We then investigated whether hnRNPA2/B1 regulates *BACE1* splicing by exposing primary hippocampal cultured neurons to lentivirus carrying shRNA against hnRNPA2B1. Our results showed changes in BACE1 splicing similar to cholinergic deficiency (Figure 2C), directly implicating hnRNPA2/B1 in the regulation of *BACE1* splicing. To test for the role of cholinergic signalling and the different cholinergic receptors in mediating this splicing event, we treated cultured

hippocampal neurons with the cholinergic mimetic carbachol. This treatment was able to decrease the proportion of BACE1-501. This decrease was blocked by co-treatment with the muscarinic antagonist atropine (Figure 2D). These data implicate muscarinic receptors in the regulation of BACE1 splicing. This splicing event in BACE1 predicts an increase in the levels of the mature BACE1 protein and indeed, immunoblot analysis revealed a 2-fold increase of BACE1 levels in the hippocampus of VAChT-deficient mice (Figure 2E).

In late onset AD BACE1 expression is upregulated (Hebert et al., 2008) and it is thought to contribute to age-dependent progression in AD pathology (Ly et al., 2013). We therefore tested for changes in APP processing in VAChT$^{Nkx2.1\text{-}Cre\text{-}flox/flox}$ mice. Aged VAChT-deficient mice (11-14 month old) displayed a modified pattern of Tris-soluble APP fragments (Figure 2F), similar to that of mouse models with APP/PS1 mutations (Jankowsky et al., 2004; Oddo et al., 2003). In contrast, membrane-bound C-terminal fragments of APP (α and β CTFs), alterations of which can suggest impaired proteolytic processing of the protein [Reviewed in (Selkoe, 2000)], were similar in VAChT-deficient mice and controls (Figure 2G). APP processing was not modified in aged Nkx2.1-Cre mice (Figure S3A), suggesting that this effect is due to cholinergic dysfunction rather than to Cre expression.

We then assessed the levels of mouse amyloid peptides using an ELISA kit validated for both mouse and human Aβ peptides (Teich et al., 2013). The hippocampus of aged VAChT$^{Nkx2.1\text{-}Cre\text{-}flox/flox}$ mice showed increased levels of soluble mouse Aβ peptide compared to controls (Figure 2H), reaching about one third of the levels of those found in aged 5XFAD mouse model of AD, which is one of the most aggressive

models of AD amyloidosis. In comparison, insoluble amyloid peptide was undetectable in the brains of VAChT-deficient mice, whereas it was highly abundant in the 5XFAD mice (Figure 2H). In addition, neither control nor VAChT-deficient mice displayed positive Congo red staining, unlike brain sections from 5XFAD mice, which exhibited numerous Congo red plaques (Figure 2I). These data indicate that although VAChT-deficient mice show increased levels of soluble Aβ peptides, they do not seem to accumulate in extracellular amyloid plaques. Indeed, the murine amyloid peptide is much less prone to aggregation than human Aβ due to two amino acid changes (Jankowsky et al., 2007).

Cholinergic deficit leads to age-dependent hippocampal tauopathy

In AD, increased levels of soluble Aβ peptides are thought to precede abnormal phosphorylation of the microtubule associated protein tau (Iqbal et al., 2010). Previous reports suggested that cholinergic activity and tau phosphorylation might be inter-related (Hellstrom-Lindahl, 2000). Therefore, we used immunofluorescence to assess levels of the AT180 tau epitope (T231/S235) in the hippocampus of VAChT-deficient mice. This phosphorylation-dependent antibody specific to pT231 has been shown to label approximately 70% of paired helical filaments (PHF) in AD brains (Goedert et al., 1994). Phosphorylation at this epitope reduces the binding of tau to microtubules potentially increasing its toxicity (Lim et al., 2008). Immunofluorescence imaging revealed a robust increase of AT180 immunoreactivity in the hippocampus of $VAChT^{Nkx2.1\text{-}Cre\text{-}flox/flox}$ mice compared to aged-matched controls (Figure 3A- 11-14 month-old mice). To test if the positive immunoreactivity of pTau in VAChT-deficient mice is associated with an induction of pathological tau, immunofluorescence with MC1

antibody was performed. Positive reactivity of conformation-dependent MC1 antibody depends on the proximity of N terminal (aa 7-9) and C-terminal (313-333) amino acid sequences of tau, which is one of the earliest alterations of tau in AD (Weaver et al., 2000; Wolozin et al., 1986). Immunostaining with MC1 revealed positive immunoreactivity in the hippocampus of aged cholinergic-deficient mice, but not in age-matched controls (Figure 3B).

In agreement with the immunofluorescence data, hippocampal extracts of VAChT$^{Nkx2.1\text{-}Cre\text{-}flox/flox}$ mice showed approximately four-fold increases in pTau immunoreactive bands, including higher order oligomers detected with AT180, when compared to controls (Figure 3C and D). On the other hand, total tau and pTauS262 levels were unmodified in VAChT-deficient mice (Figure 3C and D). Taken together, our data indicate that deletion of hippocampal VAChT induces hyper-phosphorylation of tau and leads to tau pathological conformation as detected by MC1, both of which are consistently observed in AD. These data suggest the potential for neuronal toxicity due to cholinergic dysfunction.

Cholinergic deficiency exacerbates age-dependent neuronal vulnerability and impaired learning.

Synaptic health is compromised in mouse models of AD and synaptic loss is a consistent finding in AD-affected individuals (Klein, 2006). To examine synaptic integrity we stained hippocampal sections with the synaptic marker PSD95. Aged VAChT$^{Nkx2.1\text{-}Cre\text{-}flox/flox}$ mice displayed hippocampal decreases in PSD95-immunoreactivity, increased microglial activation and up-regulation of inflammatory markers, in comparison to age-matched controls, suggesting large-scale synaptic dysfunction in these mutants (Figure

4A-C). These observations predict neuronal vulnerability; therefore, we stained brain sections with silver, which accumulates in neurons that are more vulnerable to neurodegeneration (DeOlmos and Ingram, 1971). Aged VAChT-deficient mice presented intensified silver staining compared to controls; this increased silver staining was not observed in young VAChT-deficient mice (Figure 4D-E), suggesting that long-lasting decrease in cholinergic signalling may increase the vulnerability of hippocampal neurons. Parallel staining of hippocampal sections from aged 5XFAD mice compared to control mice performed as a positive control revealed similar increases in silver staining as that for VAChT-deficient mice (Figure S4).

Activated caspase-3, a marker of apoptosis, was augmented in young VAChT$^{Nkx2.1\text{-}Cre\text{-}flox/flox}$ mice compared to controls (Figure 4F). However, aging significantly increased the number of activated caspase-positive cells in VAChT-deficient mice when compared to controls (Figure 4F). Also, young VAChT-deficient mice showed no alteration in the number of NeuN positive cells across all regions of the hippocampus (Figure 4G, Figure S4); while NeuN positive cells in CA1 and CA3 region, but not dentate gyrus were decreased in aged VAChT-deficient mice (Figure 4G, Figure S4), predicting functional implications for this aging-related hippocampal neuronal vulnerability. Thus, impaired cholinergic signalling induces global changes in transcript levels, followed by age-related exacerbation of synaptic and neuronal vulnerability.

To test whether long-lasting cholinergic failure may have age-dependent consequences in cognitive function, we subjected aged (11-14 months old) VAChT-deficient mice to the MWM task. Young VAChT-deficient mice (3-6 months old) show little difference from controls in acquisition performance on the Morris Water Maze

(MWM) task (Al-Onaizi et al., 2016). In contrast, aged VAChT-deficient mice took significantly longer and swam a greater distance than age-matched controls to find the platform across the four days of acquisition (Figure S4E-F). Furthermore, aged VAChT-deficient mice used distinct strategy preferences to find the platform, indicating that their deteriorated performance was due to modified learning capacities. Briefly, the analysis of search strategies used by each animal was based on a fixed set of criteria (Figure 4H). At a young age, both controls and VAChT$^{Nkx2.1\text{-}Cre\text{-}flox/flox}$ mice predominantly used a more direct strategy to reach the platform (strategies 5/6/7, Figure 4I). In contrast, aged VAChT-deficient mice used random swimming predominantly as their strategy to acquire the task (strategy 2, Figure 4I), while aged control mice maintained the use of more direct strategies. Aged VAChT-deficient mice also exhibited deficits in the probe trial (Figure S4G). Taken together, these results suggest that long-term cholinergic deficiency in VAChT$^{Nkx2.1\text{-}Cre\text{-}flox/flox}$ mice led to progressive loss of neurons in the hippocampus that worsened spatial information acquisition and cognitive functioning.

Cholinergic mediated age dependent pathology is partially mediated by GSK3 activation

In addition to APP processing and tau hyperphosphorylation, we observed other critical biochemical pathways altered in response to cholinergic deficiency, including aberrant GSK3 signalling, which has also been shown to play multiple roles in AD (Endo et al., 2006; Gary and Mattson, 2001). As several genes that regulate the PI3-AKT pathway were upregulated in VAChT-deficient mice (Fig. 1D, S1), we tested for dysregulation of PI3-AKT signalling pathway in these mice by evaluating the phosphorylation status of the AKT protein and its downstream target GSK3. AKT

presented decreased phosphorylation at residue Ser473, with unmodified Thr308 phosphorylation, in VAChT$^{Nkx2.1\text{-}Cre\text{-}flox/flox}$ hippocampus compared to controls (Figure 5A). Additionally, GSK3α/β tyrosine phosphorylation, which reflects activation of GSK3, was increased in these mutants (Figure 5B). Hence in addition to increased levels of proteins involved in AD pathology, these results suggest potential contributions of GSK3 activation in cholinergic-induced deficits.

To test the role of GSK3 in the abnormal hippocampal changes in cholinergic-deficient mice, we chronically treated a cohort of aged (11 months old) VAChT$^{NKx2.1\text{-}Cre\text{-}flox/flox}$ mice with the GSK3 inhibitor AR-A014418 (Figure 5C). After 28 days of treatment, we found that VAChT-deficient mice treated with AR-A014418 showed a significant decrease in GSK3 α and β tyrosine phosphorylation when compared to VAChT$^{NKx2.1\text{-}Cre\text{-}flox/flox}$ mice treated with saline (Figure 5D). Increased phosphorylation at Tyr residues 216 or 279 augments GSK3 activity (Hur and Zhou, 2010) and examining GSK3 phosphorylation at these residues has been used to determine the effectiveness of AR-A014418 (Carter et al., 2014; Yadav et al., 2014). We then assessed some of the key alterations detected in the hippocampus of aged VAChT$^{NKx2.1\text{-}Cre\text{-}flox/flox}$ mice. AR-A014418 treatment was able to significantly decrease tau T231 hyperphosphorylation and MC1-immunopositive tau in Western blots (Chai et al., 2011; Petry et al., 2014), by approximately 50% in VAChT$^{NKx2.1\text{-}Cre\text{-}flox/flox}$ mice when compared to saline VAChT$^{NKx2.1\text{-}Cre\text{-}flox/flox}$ mice. Total levels of tau where unchanged (Figure 5E). Immunofluorescence staining (Figure 5F) also demonstrated reduced levels of T231 hyperphosphorylated tau in AR-A014418 treated mice. Compared to saline treated animals, AR-A014418 treatment was able to significantly increase levels of PSD-95 protein (Figure 5G).

Interestingly, we observed no changes in protein levels of BACE1 following AR-A014418 treatment in aged VAChT$^{NKx2.1\text{-}Cre\text{-}flox/flox}$ mice (Fig.S5A). Furthermore AR-A014418 treatment did not alter the alternative splicing event in the BACE1 gene (Figure S5A). Together, these data suggest that the hnRNPA2/B1-mediated alternative splicing and subsequent increase in BACE1 protein level are not mediated by GSK3 activation. Surprisingly, despite reduced levels of hyperphosphorylated tau, 1-month AR-A014418 treatment was unable to decrease the elevated levels of activated caspase-3, (Figure S5C-D).

Cholinergic dysfunction in human AD brains

Whether cholinergic genes are expressed in lower levels in human AD brain compared to cognitively alert controls and may contribute to phenotypes detected herein is not fully understood. To examine that, we extracted total RNA from a cohort of 24 adult human temporal gyrus samples collected at the Netherland Brain Bank (sample information in Table SII), including 8 sporadic AD patients and 16 from age-matched controls. We then profiled AD-related transcript differences by adopting the particularly deep SQUARE^{TM} RNA library construction approach (Hebenstreit and Teichmann, 2011). Of those, 10,885 genes that were expressed showed a significant change. Next, we quantified the levels of those transcripts composing the expanded family of cholinergic regulator genes (Soreq, 2015). Detected cholinergic transcripts showed significantly lower expression levels than other protein-coding genes in the temporal gyrus of AD patients compared to aged-matched controls (Figure 6A).

Brain samples from a distinct cohort of AD patients (Ostapchenko et al., 2013) supported the RNA-Seq analysis results by showing a significant VAChT loss in AD

brains compared to age and sex-matched controls (Figure 6B), in agreement with previous observations (Chen et al., 2011; Efange et al., 1997). Furthermore, the cohort of AD brains exhibited 50% decrease in hnRNPA2/B1 protein levels compared to age/gender-matched controls (Figure 6C), confirming previous results obtained with a distinct AD cohort (Berson et al., 2012). Additionally, we found a significant positive correlation between VAChT and hnRNPA2/B1 protein levels (Figure 6D). AD brain samples also showed drastic increases in tau-Thr231 phosphorylation (Figure 6E), which was inversely proportional to the levels of VAChT (Figure 6F). Our findings using cholinergic-deficient mice support an intricate timeline whereby cholinergic dysfunction *per se* precedes and may have strong influence in pathological changes observed in AD.

Discussion

We employed transcriptome and biochemical assays on cholinergic-deficient mouse brain samples to explore the impact of long-lasting forebrain cholinergic dysfunction. Whole-genome RNA sequencing demonstrated that cholinergic deficiency modifies expression levels and isoform abundance of several key transcripts related to Alzheimer's disease in the hippocampus of VAChT-deficient mice. Cholinergic-mediated abnormal *BACE1* mRNA splicing in VAChT-mutant mice increased BACE1 protein levels and APP processing. Accordingly, cholinergic deficiency caused a 10-fold increase in soluble mouse Aβ peptides, age-dependent hippocampal tauopathy, synaptic abnormalities, neuronal inflammation, neuronal vulnerability and cognitive decline. We also showed that GSK3 activation is critical for cholinergic modulation of tau hyperphosphorylation and synaptic vulnerability. Furthermore, we confirmed that

human AD brains present cholinergic dysfunction and showed that it correlates to changes in the levels of hnRNP A2/B1 and hyperphosphorylated tau. Our findings indicate that cholinergic impairments confer widespread hippocampal damage and malfunction. Furthermore, our data support a causal role for cholinergic signalling as a surveillance mechanism controlling hippocampal transcript levels, maintenance of cognitive function and neuronal viability in mice.

Our RNA sequencing analysis revealed a group of differentially expressed transcripts related to spliceosome regulation in the hippocampus of VAChT$^{Nkx2.1\text{-}Cre\text{-}flox/flox}$ mice, suggesting that the splicing machinery in these mutants could be altered. In fact, a significant number of alternative splicing event abnormalities were observed in the hippocampus of VAChT-deficient mice. These results are consistent with previously reported global changes of alternative splicing in the AD brain (Bai et al., 2013; Berson et al., 2012; Tollervey et al., 2011). Importantly, spliceosome signalling pathway changes can have broad implications for gene regulation [reviewed in (Shin and Manley, 2004)].

Alternative splicing in the nervous system is particularly widespread and is essential for multiple aspects of neuronal function (Raj and Blencowe, 2015). However, the signal-transduction pathways that regulate splicing are not well known (Shin and Manley, 2004). Our study adds a role for cholinergic signalling in the maintenance of balanced alternative splicing. At least part of the cholinergic-control of alternative splicing seems to involve hnRNPA2/B1. We have shown that cholinergic deficiency in the cortex (Berson et al., 2012; Kolisnyk et al., 2013a) and hippocampus (Figure 2B) leads to decreased expression of the hnRNPA2/B1 protein. Related work demonstrated

that hnRNPA2/B1 is a cholinergic regulated splicing factor (Kolisnyk et al submitted). Importantly, knockdown of hnRNPA2/B1 in cultured hippocampal neurons shifted splicing of *BACE1* mRNA towards increased expression of mRNA species coding for the BACE1-501 protein isoform as observed in the hippocampus of *VAChT*-deficient mice. This splicing change led to increased expression of the BACE1 protein that was accompanied by a pattern of APP processing similar to that observed in commonly used mouse models of AD. The alternative splicing event in BACE1 observed in VAChT-mutant mice is regulated my M1 muscarinic receptors (Kolisnyk et al., submitted).

Cholinergic tone has been thought to regulate APP processing through muscarinic receptors (Davis et al., 2010; Nitsch et al., 1992). Specifically, M1 signalling has been shown to regulate the stability of the BACE1 protein (Davis et al., 2010). BACE1-501 is a more stable and active form of the protein (Mowrer and Wolfe, 2008). Remarkably, BACE1 expression is increased in late-onset AD (Hebert et al., 2008). Our data suggest potential mechanisms by which cholinergic regulation can affect BACE1 expression and AD pathology. Interestingly, our data suggest changes in alternative splicing occurs post-transcriptionally and independent of GSK3 signalling. Thus, cholinergic deficiency may affect BACE1 expression differently than previously described in AD, in which GSK3 can regulate BACE1 transcription by increasing promoter activity (Ly et al., 2013). Our findings promote upstream cholinergic mechanisms as a target for diminishing aberrant APP processing in AD.

In addition to increased levels of soluble Aβ, VAChT$^{Nkx2.1\text{-}Cre\text{-}flox/flox}$ mice also show tau hyper-phosphorylation, which destabilizes microtubules and significantly disrupts axonal transport. Tau hyper-phosphorylation may also contribute to increased

vulnerability leading to neuronal death (Billingsley and Kincaid, 1997). In fact, VAChT-deficient mice show age-dependent increases in hippocampal argyrophilic staining and neuronal death.

Oligomeric protein aggregation has been linked to toxicity and to neurodegenerative disorders, including AD (Maeda et al., 2006). The formation of NFTs alone is insufficient for neurodegeneration, yet oligomeric tau may contribute to neurodegeneration and synaptic loss in AD (Berger et al., 2007; de Calignon et al., 2012). These observed changes in tau in VAChT-deficient mice (i.e. increased oligomer formation), the associated age-dependent increase in immunoreactivity of activated caspase-3, and ultimately neuronal loss all support a relationship between cholinergic failure and AD-like pathology in mice.

Tau hyper-phosphorylation can occur due to the increased activity of GSK3, which subsequently leads to an array of impairments, including disruption of LTP (Hooper et al., 2007) and cell death *in vitro* (Zheng et al., 2002). GSK3 over-activation is an important hallmark in AD (Hooper et al., 2008). Thus, the GSK3 overactivation observed in VAChT-mutant mice represents a potential mechanism by which reduced cholinergic activity may have multiple influences in AD pathology in target cells. We tested this hypothesis by pharmacological inhibition of GSK3 in aged VAChT-deficient mice. GSK3 inhibition was able to decrease tau hyperphosphorylation. Also, GSK3 inhibition partially restored PSD95 protein levels, but did not decrease caspase-3 activation. These findings demonstrate that cholinergic-induced changes in tau and in amyloid processing are potentially independent of each other and suggest that cholinergic dysfunction is contributing to the pathological outcomes in these animals by

altering multiple pathways. The pharmacological inhibition of GSK3 was tested in mice in which certain pathology was already present (11-12 month-old mice). Hence, further experiments should test longer treatments with the compound or genetic ablation of GSK3 genes in VAChT-deficient mice to comprehensively dissect the contribution of overactive GSK3 in other phenotypes.

Aged VAChT-deficient mice showed a decrease in the number of hippocampal neurons, a deficiency that was not observed in young mutants, suggesting that cholinergic tone may play a role in guarding hippocampal neuronal health. Additionally, aged VAChT-deficient mice showed increased neuroinflammation and reduced number of synapses; which are pathologies observed in AD brains (DeKosky and Scheff, 1990; Rogers and Shen, 2000; Smale et al., 1995). Mice with excess acetylcholinesterase, which present decreased cholinergic function, also show neuroinflammation (Shaked et al., 2009). Furthermore, similar to our observation, mice lacking the β2 nicotinic receptor subunit show age-dependent loss of hippocampal neurons (Zoli et al., 1999). Of note, hippocampal neuronal loss is a critical feature in AD, which is not observed in mouse models overexpressing APP and or presenilin 1 with human AD mutations (Stein and Johnson, 2002). Hence, long-term cholinergic deficiency may model this aspect of AD in a better way. Potential mechanisms involved in cholinergic dysfunction induced pathology are shown on Figure 7.

In line with an age-dependent loss of hippocampal neurons, we found that aged VAChT-deficient mice showed significant impairments in their learning strategy in the MWM task. Poor performance and acquisition on the MWM task has been associated

with loss of neurons in the hippocampus (Olsen et al., 1994). This suggests that neuronal loss in the hippocampus has functional consequences in mice as well.

In AD brains, we found evidence of cholinergic decline and showed a striking relationship between VAChT levels and tau hyper-phosphorylation. Together with the mouse data, these observations support the notion that deficient cholinergic signalling in AD may correlate to key pathological events, including Tau hyper-phosphorylation.

Our data reveal that cholinergic deficiency can affect a number of transcriptional processes, disturb splicing of key genes and interfere with protein networks that normally protect neurons. Interestingly, recent work revealed that basal forebrain cholinergic neurons present intraneuronal Aβ accumulation even in young adults, which may contribute to their selective vulnerability in AD (Baker-Nigh et al., 2015). Cholinergic neurons are thought to be highly dependent on the presence of trophic factors for their optimal function and survival (Boskovic et al., 2014; Naumann et al., 2002), which may also contribute to their demise. Regardless of the mechanisms for increased cholinergic vulnerability in AD, it seems that cholinergic dysfunction persisting for a long period is highly related to hippocampal pathology and amyloid accumulation (Teipel et al., 2014).

In short, our results suggest that long-term cholinergic failure *per se*, which we model by disrupting synaptic cholinergic function, can trigger AD-like pathology in mice. More importantly, we find that long-term cholinergic deficiency leads to age-dependent cognitive decline that is related to neuronal death, a key feature of late-onset AD that is not modeled in mice overexpressing human genes with AD-related mutations. Our experiments provide a mechanism to explain how decreased cholinergic tone, for

example due to long-term use of anti-cholinergic drugs, could lead to increased risk of dementia (Gray et al., 2015), which may depend on global changes of RNA metabolism, including alternative splicing and gene expression. It remains to be determined if rescuing cholinergic function prior to development of AD could have an impact in the risk of dementia or AD-related pathology. However, it is noteworthy that recent observations in potential prodromal AD-affected individuals indicate that cholinesterase inhibition decreases the rate of hippocampal atrophy by 45% during one-year treatment (Dubois et al., 2015). Our data points towards cholinergic signalling being a global mediator of several distinct processes that when dysfunctional lead to pathology. Developing effective strategies to reverse the cholinergic deficits in the AD brain may therefore prove to be more fruitful then specific therapies based on reversing the individual processes it regulates.

Acknowledgements:

The authors declare no competing financial interests. They are grateful to Dr. David E. Greenberg, Hebrew University of Jerusalem, for fruitful discussions; to Dr. Alexander Seitz and Dr. Torsten Reda, Lexogen, Vienna, and Mr. Alessandro Guffanti, Genomnia, Milan, for technical and analytic support; the Netherland Brain bank for tissues and data; Jue Fan, Sandra Raulic and Matthew Cowan for animal care and technical support; to Dr. R. Jane Rylett (University of Western Ontario, Canada) and Dr. Peter Davies (Albert Einstein College of Medicine of Yeshiva University, USA) for providing antibodies; and to the Center for Applied Genomics, SickKids, Toronto for RNA-Seq experiments. This work was supported by the Canadian Institute of Health Research

(MOP 93651, MOP 136930, MOP 126000 and MOP 89919), NSERC (402524-2013), Brain Canada, Canadian Foundation for Innovation, and Ontario research fund (M.A.M.P. And V.F.P.). H.S acknowledges support by the European Research Council (Advanced Award 321501), and the Legacy Heritage Science Initiative (LHSI) of the Israel Science Foundation (Grant No. 378/11). S.B. is an incumbent of the TEVA National Network of Excellence in Neuroscience – NNE fellowship. B.K. is a recipient of the Annie Darkens Research Fund Award from the Alzheimer's Society of Canada fellowship and M.A.A-O received fellowship support from Kuwait University. JSS received a fellowship from the Science without borders program (Brazil). L.S. was funded by a Marie Curie Actions Intra European Fellowship, the European Commission (call FP7-PEOPLE-2013-IEF, project: PRANA).

Author contributions

B.K., M.A.A-O., L.S., J.U., H.S., V.F.P., M.A.M.P. designed experiments; B.K., M.A.A-O., L.S., S.B., G.H., U.B., J.X., G.M.P., M.T. K., J.S.S. conducted experiments; M.F. Contributed with materials; B.K., M.A.A-O, L.S., S.B., G.H., U.B., J. U. analysed data; B.K., M.A.A-O, H.S., V.F.P., M.A.M.P. wrote the manuscript. All authors read and approved the manuscript.

Conflict of Interest

The authors declare no conflicts of interest.

References

Al-Onaizi, M.A., Parfitt, G.M., Kolisnyk, B., Law, C.S., Guzman, M.S., Barros, D.M., Leung, L.S., Prado, M.A., and Prado, V.F. (2016). Regulation of Cognitive Processing by Hippocampal Cholinergic Tone. Cerebral cortex.

Anders, S., and Huber, W. (2010). Differential expression analysis for sequence count data. Genome biology 11, R106.

Bai, B., Hales, C.M., Chen, P.C., Gozal, Y., Dammer, E.B., Fritz, J.J., Wang, X., Xia, Q., Duong, D.M., Street, C.*, et al.* (2013). U1 small nuclear ribonucleoprotein complex and RNA splicing alterations in Alzheimer's disease. Proceedings of the National Academy of Sciences of the United States of America 110, 16562-16567.

Baker-Nigh, A., Vahedi, S., Davis, E.G., Weintraub, S., Bigio, E.H., Klein, W.L., and Geula, C. (2015). Neuronal amyloid-beta accumulation within cholinergic basal forebrain in ageing and Alzheimer's disease. Brain : a journal of neurology 138, 1722-1737.

Bartus, R.T., Dean, R.L., 3rd, Beer, B., and Lippa, A.S. (1982). The cholinergic hypothesis of geriatric memory dysfunction. Science 217, 408-414.

Beauquis, J., Vinuesa, A., Pomilio, C., Pavia, P., Galvan, V., and Saravia, F. (2014). Neuronal and glial alterations, increased anxiety, and cognitive impairment before hippocampal amyloid deposition in PDAPP mice, model of Alzheimer's disease. Hippocampus 24, 257-269.

Bekenstein, U., and Soreq, H. (2013). Heterogeneous nuclear ribonucleoprotein A1 in health and neurodegenerative disease: from structural insights to post-transcriptional regulatory roles. Molecular and cellular neurosciences 56, 436-446.

Berger, Z., Roder, H., Hanna, A., Carlson, A., Rangachari, V., Yue, M., Wszolek, Z., Ashe, K., Knight, J., Dickson, D.*, et al.* (2007). Accumulation of pathological tau species and memory loss in a conditional model of tauopathy. The Journal of neuroscience : the official journal of the Society for Neuroscience 27, 3650-3662.

Berson, A., Barbash, S., Shaltiel, G., Goll, Y., Hanin, G., Greenberg, D.S., Ketzef, M., Becker, A.J., Friedman, A., and Soreq, H. (2012). Cholinergic-associated loss of hnRNP-A/B in Alzheimer's disease impairs cortical splicing and cognitive function in mice. EMBO Mol Med 4, 730-742.

Billingsley, M.L., and Kincaid, R.L. (1997). Regulated phosphorylation and dephosphorylation of tau protein: effects on microtubule interaction, intracellular trafficking and neurodegeneration. The Biochemical journal 323 (Pt 3), 577-591.

Bindea, G., Mlecnik, B., Hackl, H., Charoentong, P., Tosolini, M., Kirilovsky, A., Fridman, W.H., Pages, F., Trajanoski, Z., and Galon, J. (2009). ClueGO: a Cytoscape plug-in to decipher functionally grouped gene ontology and pathway annotation networks. Bioinformatics 25, 1091-1093.

Boskovic, Z., Alfonsi, F., Rumballe, B.A., Fonseka, S., Windels, F., and Coulson, E.J. (2014). The role of p75NTR in cholinergic basal forebrain structure and function. The Journal of neuroscience : the official journal of the Society for Neuroscience 34, 13033-13038.

Carter, Y.M., Kunnimalaiyaan, S., Chen, H., Gamblin, T.C., and Kunnimalaiyaan, M. (2014). Specific glycogen synthase kinase-3 inhibition reduces neuroendocrine markers and suppresses neuroblastoma cell growth. Cancer biology & therapy 15, 510-515.

Chai, X., Wu, S., Murray, T.K., Kinley, R., Cella, C.V., Sims, H., Buckner, N., Hanmer, J., Davies, P., O'Neill, M.J., *et al.* (2011). Passive immunization with anti-Tau antibodies in two transgenic models: reduction of Tau pathology and delay of disease progression. The Journal of biological chemistry 286, 34457-34467.

Chen, K.H., Reese, E.A., Kim, H.W., Rapoport, S.I., and Rao, J.S. (2011). Disturbed neurotransmitter transporter expression in Alzheimer's disease brain. Journal of Alzheimer's disease : JAD 26, 755-766.

Davis, A.A., Fritz, J.J., Wess, J., Lah, J.J., and Levey, A.I. (2010). Deletion of M1 muscarinic acetylcholine receptors increases amyloid pathology in vitro and in vivo. The Journal of neuroscience : the official journal of the Society for Neuroscience 30, 4190-4196.

de Calignon, A., Polydoro, M., Suarez-Calvet, M., William, C., Adamowicz, D.H., Kopeikina, K.J., Pitstick, R., Sahara, N., Ashe, K.H., Carlson, G.A., *et al.* (2012). Propagation of tau pathology in a model of early Alzheimer's disease. Neuron 73, 685-697.

de Castro, B.M., De Jaeger, X., Martins-Silva, C., Lima, R.D., Amaral, E., Menezes, C., Lima, P., Neves, C.M., Pires, R.G., Gould, T.W., *et al.* (2009). The vesicular acetylcholine transporter is required for neuromuscular development and function. Mol Cell Biol 29, 5238-5250.

DeKosky, S.T., and Scheff, S.W. (1990). Synapse loss in frontal cortex biopsies in Alzheimer's disease: correlation with cognitive severity. Annals of neurology 27, 457-464.

DeOlmos, J.S., and Ingram, W.R. (1971). An improved cupric-silver method for impregnation of axonal and terminal degeneration. Brain research 33, 523-529.

Dewachter, I., Reverse, D., Caluwaerts, N., Ris, L., Kuiperi, C., Van den Haute, C., Spittaels, K., Umans, L., Serneels, L., Thiry, E., *et al.* (2002). Neuronal deficiency of presenilin 1 inhibits amyloid plaque formation and corrects hippocampal long-term potentiation but not a cognitive defect of amyloid precursor protein [V717I] transgenic mice. The Journal of neuroscience : the official journal of the Society for Neuroscience 22, 3445-3453.

Dubois, B., Chupin, M., Hampel, H., Lista, S., Cavedo, E., Croisile, B., Louis Tisserand, G., Touchon, J., Bonafe, A., Ousset, P.J., *et al.* (2015). Donepezil decreases annual rate of hippocampal atrophy in suspected prodromal Alzheimer's disease. Alzheimer's & dementia : the journal of the Alzheimer's Association 11, 1041-1049.

Eden, E., Navon, R., Steinfeld, I., Lipson, D., and Yakhini, Z. (2009). GOrilla: a tool for discovery and visualization of enriched GO terms in ranked gene lists. BMC bioinformatics 10, 48.

Efange, S.M., Garland, E.M., Staley, J.K., Khare, A.B., and Mash, D.C. (1997). Vesicular acetylcholine transporter density and Alzheimer's disease. Neurobiology of aging 18, 407-413.

Endo, H., Nito, C., Kamada, H., Nishi, T., and Chan, P.H. (2006). Activation of the Akt/GSK3beta signaling pathway mediates survival of vulnerable hippocampal neurons after transient global cerebral ischemia in rats. Journal of cerebral blood flow and metabolism : official journal of the International Society of Cerebral Blood Flow and Metabolism 26, 1479-1489.

Garthe, A., Behr, J., and Kempermann, G. (2009). Adult-generated hippocampal neurons allow the flexible use of spatially precise learning strategies. PloS one 4, e5464.

Gary, D.S., and Mattson, M.P. (2001). Integrin signaling via the PI3-kinase-Akt pathway increases neuronal resistance to glutamate-induced apoptosis. Journal of neurochemistry 76, 1485-1496.

Goedert, M., Jakes, R., Crowther, R.A., Cohen, P., Vanmechelen, E., Vandermeeren, M., and Cras, P. (1994). Epitope mapping of monoclonal antibodies to the paired helical filaments of Alzheimer's disease: identification of phosphorylation sites in tau protein. The Biochemical journal 301 (Pt 3), 871-877.

Gray, S.L., Anderson, M.L., Dublin, S., Hanlon, J.T., Hubbard, R., Walker, R., Yu, O., Crane, P.K., and Larson, E.B. (2015). Cumulative use of strong anticholinergics and incident dementia: a prospective cohort study. JAMA internal medicine 175, 401-407.

Grothe, M., Heinsen, H., and Teipel, S. (2013). Longitudinal measures of cholinergic forebrain atrophy in the transition from healthy aging to Alzheimer's disease. Neurobiology of aging 34, 1210-1220.
Grothe, M.J., Ewers, M., Krause, B., Heinsen, H., Teipel, S.J., and Alzheimer's Disease Neuroimaging, I. (2014). Basal forebrain atrophy and cortical amyloid deposition in nondemented elderly subjects. Alzheimer's & dementia : the journal of the Alzheimer's Association 10, S344-353.
Guzman, M.S., De Jaeger, X., Raulic, S., Souza, I.A., Li, A.X., Schmid, S., Menon, R.S., Gainetdinov, R.R., Caron, M.G., Bartha, R*., et al.* (2011). Elimination of the vesicular acetylcholine transporter in the striatum reveals regulation of behaviour by cholinergic-glutamatergic co-transmission. PLoS Biol 9, e1001194.
Hebenstreit, D., and Teichmann, S.A. (2011). Analysis and simulation of gene expression profiles in pure and mixed cell populations. Physical biology 8, 035013.
Hebert, S.S., Horre, K., Nicolai, L., Papadopoulou, A.S., Mandemakers, W., Silahtaroglu, A.N., Kauppinen, S., Delacourte, A., and De Strooper, B. (2008). Loss of microRNA cluster miR-29a/b-1 in sporadic Alzheimer's disease correlates with increased BACE1/beta-secretase expression. Proceedings of the National Academy of Sciences of the United States of America 105, 6415-6420.
Hellstrom-Lindahl, E. (2000). Modulation of beta-amyloid precursor protein processing and tau phosphorylation by acetylcholine receptors. European journal of pharmacology 393, 255-263.
Hooper, C., Killick, R., and Lovestone, S. (2008). The GSK3 hypothesis of Alzheimer's disease. Journal of neurochemistry 104, 1433-1439.
Hooper, C., Markevich, V., Plattner, F., Killick, R., Schofield, E., Engel, T., Hernandez, F., Anderton, B., Rosenblum, K., Bliss, T*., et al.* (2007). Glycogen synthase kinase-3 inhibition is integral to long-term potentiation. The European journal of neuroscience 25, 81-86.
Hur, E.M., and Zhou, F.Q. (2010). GSK3 signalling in neural development. Nature reviews Neuroscience 11, 539-551.
Iqbal, K., Liu, F., Gong, C.X., and Grundke-Iqbal, I. (2010). Tau in Alzheimer disease and related tauopathies. Current Alzheimer research 7, 656-664.
Jankowsky, J.L., Fadale, D.J., Anderson, J., Xu, G.M., Gonzales, V., Jenkins, N.A., Copeland, N.G., Lee, M.K., Younkin, L.H., Wagner, S.L*., et al.* (2004). Mutant presenilins specifically elevate the levels of the 42 residue beta-amyloid peptide in vivo: evidence for augmentation of a 42-specific gamma secretase. Human molecular genetics 13, 159-170.
Jankowsky, J.L., Younkin, L.H., Gonzales, V., Fadale, D.J., Slunt, H.H., Lester, H.A., Younkin, S.G., and Borchelt, D.R. (2007). Rodent A beta modulates the solubility and distribution of amyloid deposits in transgenic mice. The Journal of biological chemistry 282, 22707-22720.
Klein, W.L. (2006). Synaptic targeting by A beta oligomers (ADDLS) as a basis for memory loss in early Alzheimer's disease. Alzheimer's & dementia : the journal of the Alzheimer's Association 2, 43-55.
Kolisnyk, B., Al-Onaizi, M.A., Hirata, P.H., Guzman, M.S., Nikolova, S., Barbash, S., Soreq, H., Bartha, R., Prado, M.A., and Prado, V.F. (2013a). Forebrain deletion of the vesicular acetylcholine transporter results in deficits in executive function, metabolic, and RNA splicing abnormalities in the prefrontal cortex. The Journal of neuroscience : the official journal of the Society for Neuroscience 33, 14908-14920.
Kolisnyk, B., Guzman, M.S., Raulic, S., Fan, J., Magalhaes, A.C., Feng, G., Gros, R., Prado, V.F., and Prado, M.A. (2013b). ChAT-ChR2-EYFP mice have enhanced motor endurance but show deficits in attention and several additional cognitive domains. The Journal of neuroscience : the official journal of the Society for Neuroscience 33, 10427-10438.
Lim, J., Balastik, M., Lee, T.H., Nakamura, K., Liou, Y.C., Sun, A., Finn, G., Pastorino, L., Lee, V.M., and Lu, K.P. (2008). Pin1 has opposite effects on wild-type and P301L tau stability and tauopathy. The Journal of clinical investigation 118, 1877-1889.

Lima Rde, F., Prado, V.F., Prado, M.A., and Kushmerick, C. (2010). Quantal release of acetylcholine in mice with reduced levels of the vesicular acetylcholine transporter. Journal of neurochemistry 113, 943-951.

Luo, Y., Bolon, B., Kahn, S., Bennett, B.D., Babu-Khan, S., Denis, P., Fan, W., Kha, H., Zhang, J., Gong, Y., *et al.* (2001). Mice deficient in BACE1, the Alzheimer's beta-secretase, have normal phenotype and abolished beta-amyloid generation. Nature neuroscience 4, 231-232.

Ly, P.T., Wu, Y., Zou, H., Wang, R., Zhou, W., Kinoshita, A., Zhang, M., Yang, Y., Cai, F., Woodgett, J., and Song, W. (2013). Inhibition of GSK3beta-mediated BACE1 expression reduces Alzheimer-associated phenotypes. The Journal of clinical investigation 123, 224-235.

Maeda, S., Sahara, N., Saito, Y., Murayama, S., Ikai, A., and Takashima, A. (2006). Increased levels of granular tau oligomers: an early sign of brain aging and Alzheimer's disease. Neuroscience research 54, 197-201.

Martyn, A.C., De Jaeger, X., Magalhaes, A.C., Kesarwani, R., Goncalves, D.F., Raulic, S., Guzman, M.S., Jackson, M.F., Izquierdo, I., Macdonald, J.F., *et al.* (2012). Elimination of the vesicular acetylcholine transporter in the forebrain causes hyperactivity and deficits in spatial memory and long-term potentiation. Proceedings of the National Academy of Sciences of the United States of America 109, 17651-17656.

Mowrer, K.R., and Wolfe, M.S. (2008). Promotion of BACE1 mRNA alternative splicing reduces amyloid beta-peptide production. The Journal of biological chemistry 283, 18694-18701.

Naumann, T., Casademunt, E., Hollerbach, E., Hofmann, J., Dechant, G., Frotscher, M., and Barde, Y.A. (2002). Complete deletion of the neurotrophin receptor p75NTR leads to long-lasting increases in the number of basal forebrain cholinergic neurons. The Journal of neuroscience : the official journal of the Society for Neuroscience 22, 2409-2418.

Nitsch, R.M., Slack, B.E., Wurtman, R.J., and Growdon, J.H. (1992). Release of Alzheimer amyloid precursor derivatives stimulated by activation of muscarinic acetylcholine receptors. Science 258, 304-307.

Oddo, S., Caccamo, A., Shepherd, J.D., Murphy, M.P., Golde, T.E., Kayed, R., Metherate, R., Mattson, M.P., Akbari, Y., and LaFerla, F.M. (2003). Triple-transgenic model of Alzheimer's disease with plaques and tangles: intracellular Abeta and synaptic dysfunction. Neuron 39, 409-421.

Olsen, G.M., Scheel-Kruger, J., Moller, A., and Jensen, L.H. (1994). Relation of spatial learning of rats in the Morris water maze task to the number of viable CA1 neurons following four-vessel occlusion. Behavioral neuroscience 108, 681-690.

Ostapchenko, V.G., Beraldo, F.H., Mohammad, A.H., Xie, Y.F., Hirata, P.H., Magalhaes, A.C., Lamour, G., Li, H., Maciejewski, A., Belrose, J.C., *et al.* (2013). The prion protein ligand, stress-inducible phosphoprotein 1, regulates amyloid-beta oligomer toxicity. The Journal of neuroscience : the official journal of the Society for Neuroscience 33, 16552-16564.

Paz, I., Kosti, I., Ares, M., Jr., Cline, M., and Mandel-Gutfreund, Y. (2014). RBPmap: a web server for mapping binding sites of RNA-binding proteins. Nucleic acids research 42, W361-367.

Petry, F.R., Pelletier, J., Bretteville, A., Morin, F., Calon, F., Hebert, S.S., Whittington, R.A., and Planel, E. (2014). Specificity of anti-tau antibodies when analyzing mice models of Alzheimer's disease: problems and solutions. PloS one 9, e94251.

Prado, V.F., Martins-Silva, C., de Castro, B.M., Lima, R.F., Barros, D.M., Amaral, E., Ramsey, A.J., Sotnikova, T.D., Ramirez, M.R., Kim, H.G., *et al.* (2006). Mice deficient for the vesicular acetylcholine transporter are myasthenic and have deficits in object and social recognition. Neuron 51, 601-612.

Prado, V.F., Roy, A., Kolisnyk, B., Gros, R., and Prado, M.A. (2013). Regulation of cholinergic activity by the vesicular acetylcholine transporter. The Biochemical journal 450, 265-274.

Raj, B., and Blencowe, B.J. (2015). Alternative Splicing in the Mammalian Nervous System: Recent Insights into Mechanisms and Functional Roles. Neuron 87, 14-27.

Rogers, J., and Shen, Y. (2000). A perspective on inflammation in Alzheimer's disease. Annals of the New York Academy of Sciences 924, 132-135.
Selkoe, D.J. (2000). Toward a comprehensive theory for Alzheimer's disease. Hypothesis: Alzheimer's disease is caused by the cerebral accumulation and cytotoxicity of amyloid beta-protein. Annals of the New York Academy of Sciences 924, 17-25.
Shaked, I., Meerson, A., Wolf, Y., Avni, R., Greenberg, D., Gilboa-Geffen, A., and Soreq, H. (2009). MicroRNA-132 potentiates cholinergic anti-inflammatory signaling by targeting acetylcholinesterase. Immunity 31, 965-973.
Shin, C., and Manley, J.L. (2004). Cell signalling and the control of pre-mRNA splicing. Nature reviews Molecular cell biology 5, 727-738.
Smale, G., Nichols, N.R., Brady, D.R., Finch, C.E., and Horton, W.E., Jr. (1995). Evidence for apoptotic cell death in Alzheimer's disease. Experimental neurology 133, 225-230.
Soreq, H. (2015). Checks and balances on cholinergic signaling in brain and body function. Trends in neurosciences 38, 448-458.
Soreq, L., Guffanti, A., Salomonis, N., Simchovitz, A., Israel, Z., Bergman, H., and Soreq, H. (2014). Long non-coding RNA and alternative splicing modulations in Parkinson's leukocytes identified by RNA sequencing. PLoS Comput Biol 10, e1003517.
Stein, T.D., and Johnson, J.A. (2002). Lack of neurodegeneration in transgenic mice overexpressing mutant amyloid precursor protein is associated with increased levels of transthyretin and the activation of cell survival pathways. The Journal of neuroscience : the official journal of the Society for Neuroscience 22, 7380-7388.
Sun, A., Nguyen, X.V., and Bing, G. (2002). Comparative analysis of an improved thioflavin-s stain, Gallyas silver stain, and immunohistochemistry for neurofibrillary tangle demonstration on the same sections. The journal of histochemistry and cytochemistry : official journal of the Histochemistry Society 50, 463-472.
Teich, A.F., Patel, M., and Arancio, O. (2013). A reliable way to detect endogenous murine beta-amyloid. PloS one 8, e55647.
Teipel, S., Heinsen, H., Amaro, E., Jr., Grinberg, L.T., Krause, B., Grothe, M., and Alzheimer's Disease Neuroimaging, I. (2014). Cholinergic basal forebrain atrophy predicts amyloid burden in Alzheimer's disease. Neurobiology of aging 35, 482-491.
Thompson, D.F., and Walker, C.K. (2015). A descriptive and historical review of bibliometrics with applications to medical sciences. Pharmacotherapy 35, 551-559.
Tollervey, J.R., Wang, Z., Hortobagyi, T., Witten, J.T., Zarnack, K., Kayikci, M., Clark, T.A., Schweitzer, A.C., Rot, G., Curk, T.*, et al.* (2011). Analysis of alternative splicing associated with aging and neurodegeneration in the human brain. Genome research 21, 1572-1582.
Vorhees, C.V., and Williams, M.T. (2006). Morris water maze: procedures for assessing spatial and related forms of learning and memory. Nature protocols 1, 848-858.
Weaver, C.L., Espinoza, M., Kress, Y., and Davies, P. (2000). Conformational change as one of the earliest alterations of tau in Alzheimer's disease. Neurobiology of aging 21, 719-727.
Whitehouse, P.J., Price, D.L., Struble, R.G., Clark, A.W., Coyle, J.T., and Delon, M.R. (1982). Alzheimer's disease and senile dementia: loss of neurons in the basal forebrain. Science 215, 1237-1239.
Wolozin, B.L., Pruchnicki, A., Dickson, D.W., and Davies, P. (1986). A neuronal antigen in the brains of Alzheimer patients. Science 232, 648-650.
Yadav, A.K., Vashishta, V., Joshi, N., and Taneja, P. (2014). AR-A 014418 Used against GSK3beta Downregulates Expression of hnRNPA1 and SF2/ASF Splicing Factors. Journal of oncology 2014, 695325.
Zheng, W.H., Kar, S., and Quirion, R. (2002). Insulin-like growth factor-1-induced phosphorylation of transcription factor FKHRL1 is mediated by phosphatidylinositol 3-kinase/Akt kinase and role of this

pathway in insulin-like growth factor-1-induced survival of cultured hippocampal neurons. Molecular pharmacology 62, 225-233.

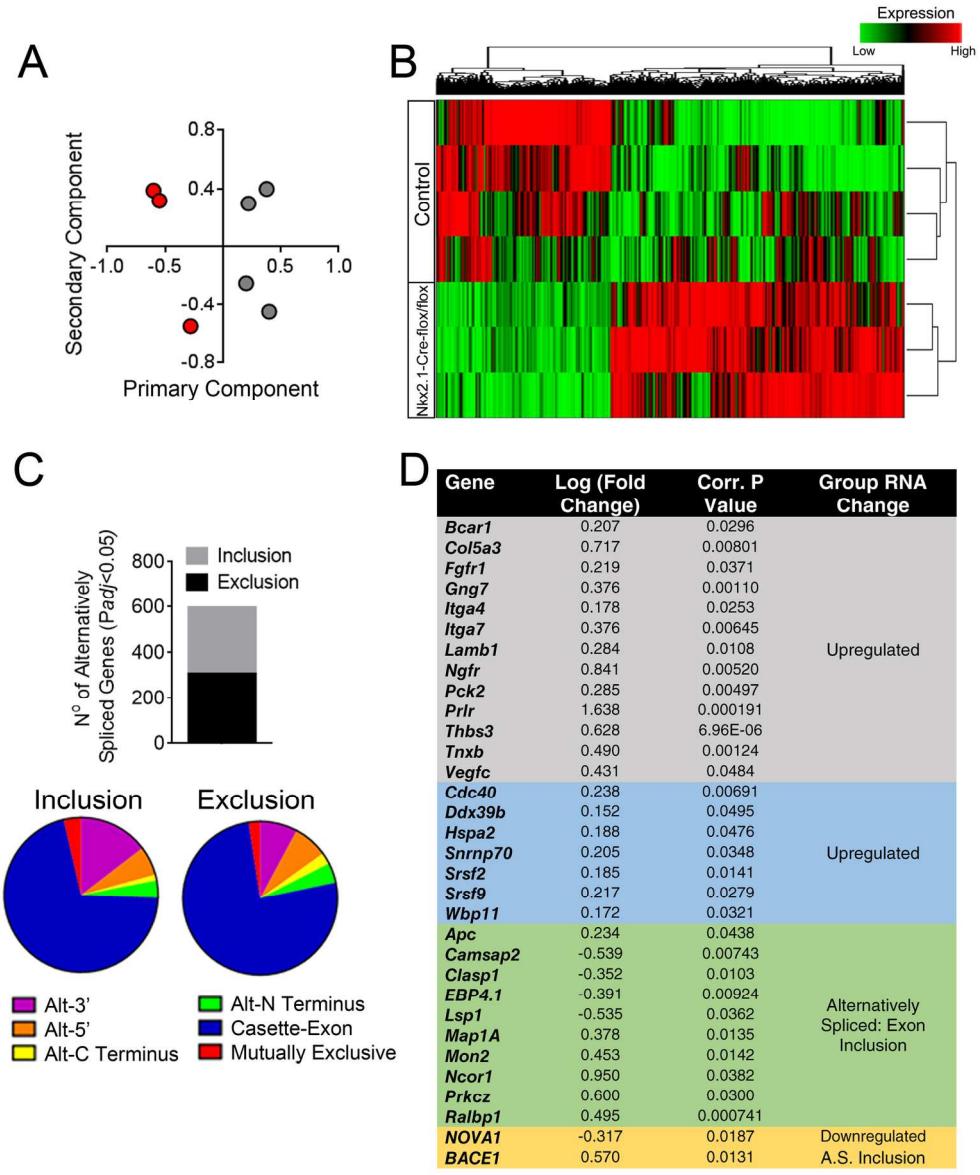

Gene	Log (Fold Change)	Corr. P Value	Group RNA Change
Bcar1	0.207	0.0296	
Col5a3	0.717	0.00801	
Fgfr1	0.219	0.0371	
Gng7	0.376	0.00110	
Itga4	0.178	0.0253	
Itga7	0.376	0.00645	
Lamb1	0.284	0.0108	Upregulated
Ngfr	0.841	0.00520	
Pck2	0.285	0.00497	
Prlr	1.638	0.000191	
Thbs3	0.628	6.96E-06	
Tnxb	0.490	0.00124	
Vegfc	0.431	0.0484	
Cdc40	0.238	0.00691	
Ddx39b	0.152	0.0495	
Hspa2	0.188	0.0476	
Snrnp70	0.205	0.0348	Upregulated
Srsf2	0.185	0.0141	
Srsf9	0.217	0.0279	
Wbp11	0.172	0.0321	
Apc	0.234	0.0438	
Camsap2	-0.539	0.00743	
Clasp1	-0.352	0.0103	
EBP4.1	-0.391	0.00924	
Lsp1	-0.535	0.0362	Alternatively Spliced: Exon Inclusion
Map1A	0.378	0.0135	
Mon2	0.453	0.0142	
Ncor1	0.950	0.0382	
Prkcz	0.600	0.0300	
Ralbp1	0.495	0.000741	
NOVA1	-0.317	0.0187	Downregulated A.S. Inclusion
BACE1	0.570	0.0131	

Figure 1. Forebrain deletion of VAChT induces alterations in hippocampal transcriptome. (A) Principal component analysis of transcripts from the hippocampi of control (VAChTflox/flox; gray circles) and VAChTNKx2.1-Cre-flox/flox (red circles) mice. (B) Cluster analysis of differentially regulated transcripts in the hippocampus of VAChTNKx2.1-Cre-flox/flox (n=3) mice compared to controls (n=4). (C) Number of genes at indicated significance cut-off that were found to have an exon inclusion or exclusion event and summary of alternative splicing events. (D) List of genes from the PI3K-AKT pathway (grey shading), Spliceosome pathway (blue shading), Microtubule polymerization pathway (green shading) and other AD genes of interest (yellow shading), identified from KEGG pathway analysis of altered transcripts in VAChTNKx2.1-Cre-flox/flox mice. For each gene corresponding fold change, corrected statistical significance levels, and RNA expression change is also shown. Altered mRNA expression of these genes has been confirmed by qPCR (see Fig. S1).
166x198mm (300 x 300 DPI)

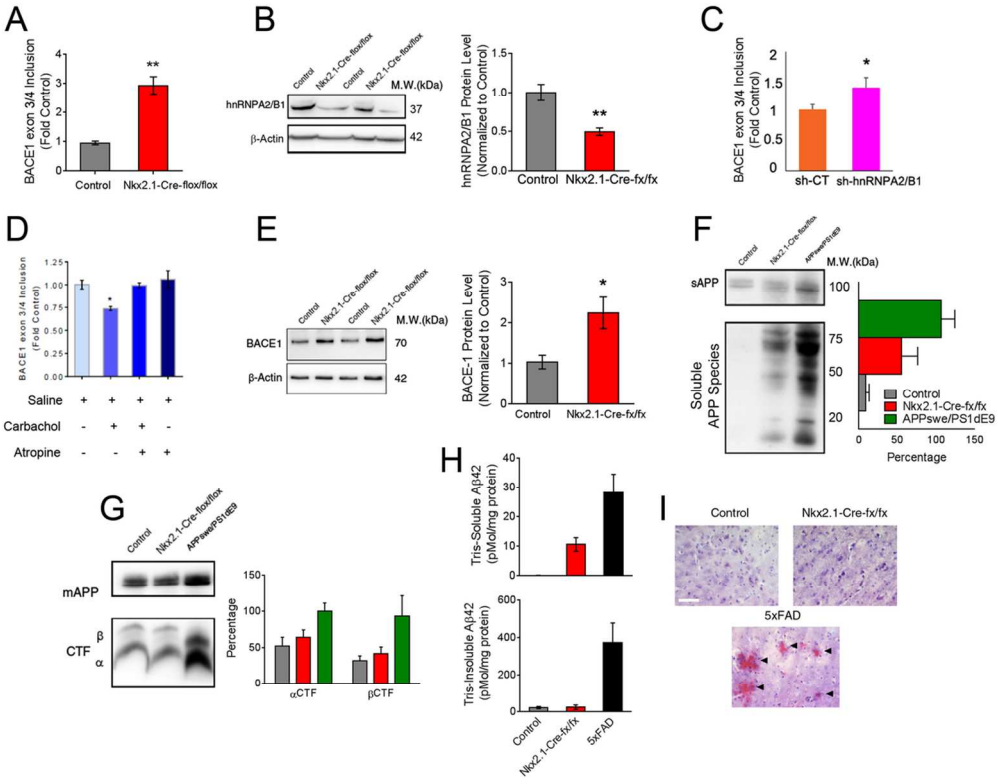

Figure 2. Disrupted APP processing and alternative splicing of BACE1 in cholinergic deficient mice. (A) qPCR analysis of alternative splicing events for BACE1 in the hippocampus of controls and (VAChTflox/flox; gray bars) and VAChTNKx2.1-Cre-flox/flox (red bars). Alternative exon levels are normalized to a constitutive exon from the same gene (n=6, data are mean ± SEM. **P<0.01). (B) Representative Western blot and quantification of hnRNPA2/B1 protein expression in the hippocampus of controls (VAChTflox/flox; gray bars) and VAChTNKx2.1-Cre-flox/flox (red bars) mice. hnRNPA2/B1 expression was normalized to actin (n=4, data are mean ± SEM. **P<0.01). (C) Quantification of the BACE1 alternative splicing in primary neuron cultures treated with hnRNPA2B1-shRNA (*P<0.05). (D) Quantification of the BACE1 alternative splicing in primary neuron cultures treated with 10mM Carbachol and Atropine (n=4, data are mean ± SEM. **P<0.05). (E) Representative Western blot and quantification of BACE1 protein levels in the hippocampus of controls (VAChTflox/flox; gray bars) and VAChTNKx2.1-Cre-flox/flox (red bars) mice. BACE1 expression was normalized to actin (n=3, data are mean ± SEM. *P<0.05). (F) Biochemical analysis and quantification of murine APP fragments in brain homogenates of aged expressed as a % [(Signal intensity of the fragment/signal intensity of full-length protein) x100]. 11-14 month old controls (VAChTflox/flox; gray bars), VAChTNKx2.1-Cre-flox/flox (red bars) and APPswe/PS1dE9 (green bars) hippocampal tissue extracts were resolved by Western blotting (data are mean ± SEM n=3). (G) Analysis of membrane-bound APP fragments in aged controls (VAChTflox/flox; gray bars) and VAChTNKx2.1-Cre-flox/flox (red bars) and APPswe/PS1dE9 (green bars) (data are mean ± SEM n=3). (H) Murine soluble and insoluble levels of Aβ42 in aged (11-14 months old) controls (VAChTflox/flox; gray bars), VAChTNKx2.1-Cre-flox/flox (red bars) and 5xFAD (black bars) measured by ELISA (n=4) (I) Congo red staining in the CA1 region of the hippocampus in aged (11-14 months old) controls, VAChTNKx2.1-Cre-flox/flox, and 5xFAD mice. Arrowheads indicate positive-Congo red staining suggestive of amyloid plaques. (n=3, Scale bar, 100μm).
113x88mm (300 x 300 DPI)

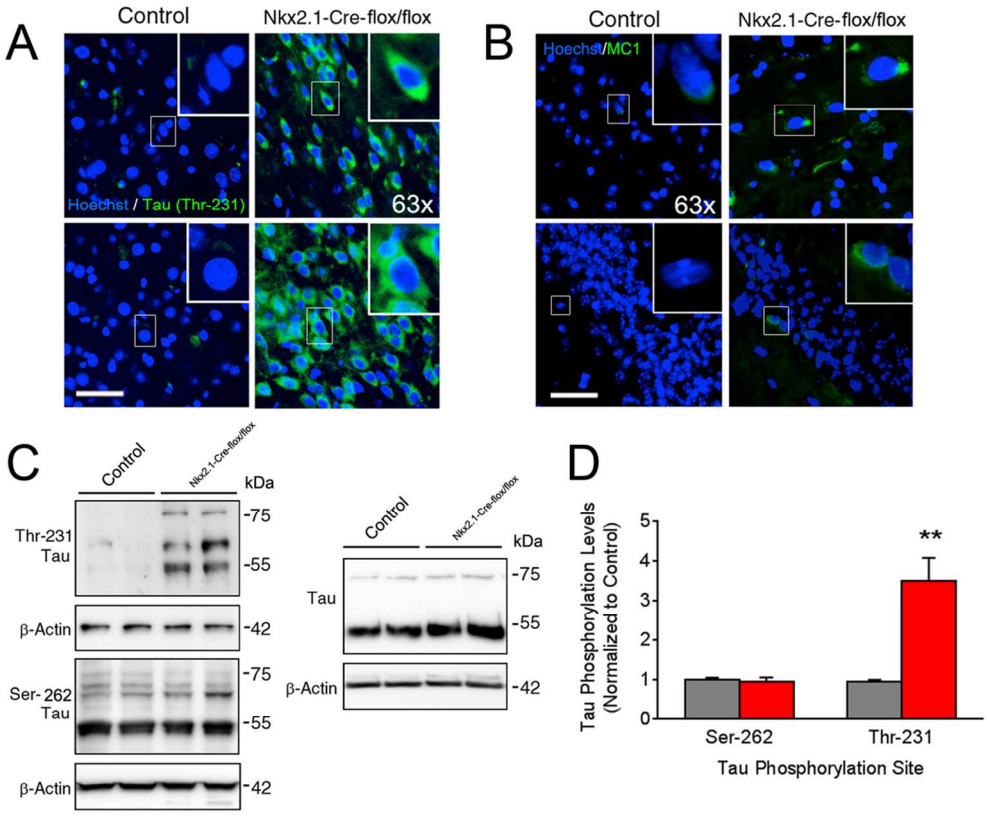

Figure 3. Hippocampal cholinergic failure triggers tauopathy in an age-dependent manner. (A) Phosphorylated Tau levels monitored by immunolabeling with phosphorylation-dependent antibodies specific to pT231. Representative images of pT231 and Hoeschst labeling in the hippocampus of aged (11-14 month old) controls (left) and VAChTNKx2.1-Cre-flox/flox (right) mice. (n=3, Scale bar, 100μm). (B) Representative images of MC1 and Hoeschst labeling in the CA1 region of the hippocampus of controls (left) and VAChTNKx2.1-Cre-flox/flox (right) mice. (n=3, Scale bar, 100μm). (C) Western blot analysis of controls (VAChTflox/flox) and VAChTNKx2.1-Cre-flox/flox aged (11-14 month old) hippocampal samples for tau using phosphorylation-dependent anti-tau antibodies pT231, Ser 262 and for total Tau protein expression. (D) Quantification of Western blots. pT231, Ser 262, and total tau expression were normalized to actin (n= 4, data are mean ± SEM. **P<0.01).
103x84mm (300 x 300 DPI)

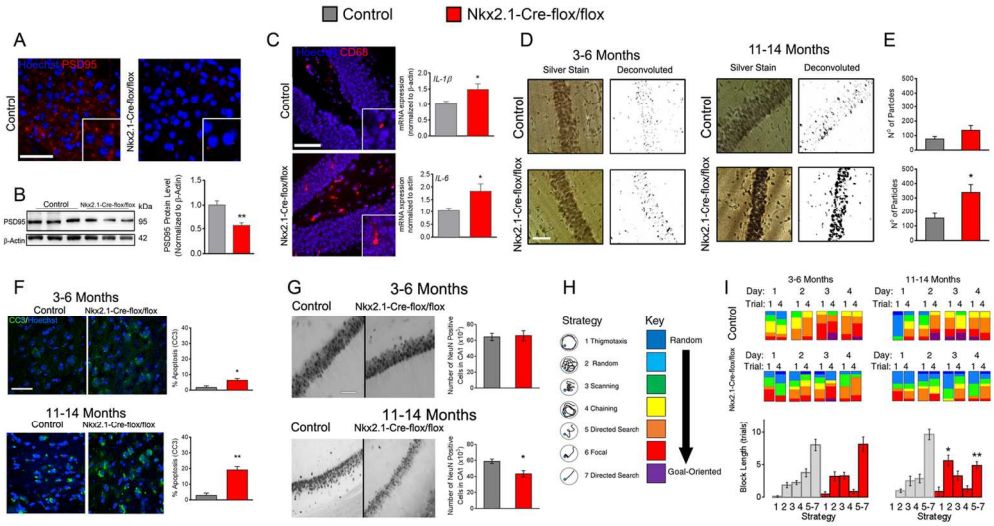

Figure 4. Hippocampal cholinergic failure leads to increased neuronal vulnerability and worsens cognitive functioning. (A) Immunofluorescence imaging showing PSD-95 protein levels in the hippocampus of aged controls or VAChTNkx2.1-Cre-flox/flox mice and corresponding (B) Western blot analysis for PSD-95 protein levels in the hippocampus of VAChTNkx2.1-Cre-flox/flox mice compared to controls ($t(6)=4.286$, $p=0.0052$, $n=4$). (C) Immunofluorescence imaging and quantification showing CD-68 immunoreactivity in the hippocampus of aged VAChTNkx2.1-Cre-flox/flox mice as well as levels of IL-1 transcripts as measured by qRT-PCR ($t(10)=2.312$, $p=0.0434$, $n=6$) and IL-6 transcripts as measured by qRT-PCR ($t(10)=2.882$, $p=0.0204$) (Data are mean +/- S.E.M., *$P<0.05$, $n=6$). (D) Representative images of silver staining in the CA1 region of young (3-6 months) and aged (11-14 months) mice. Scale bar, 100µm. (E) Quantification of silver stain-positive cells between young and aged hippocampi of controls (VAChTflox/flox; gray bars) and VAChTNKx2.1-Cre-flox/flox (red bars). (n=5, data are mean ± SEM. **$P<0.01$). (F) Representative immunofluorescence images for activated-caspase 3 labelling in the hippocampi of young (Top) and aged (Bottom) mice. Quantification of activated caspase-3 immunolabelling in young and aged hippocampi of controls (VAChTflox/flox; gray bars) and VAChTNKx2.1-Cre-flox/flox (red bars). (n= 3, data are mean ± SEM. *$P<0.05$, **$P<0.01$, Scale bar, 100µm). (G) Distribution of neuron-specific nuclear antigen (NeuN)-positive neurons in the CA1 region of the hippocampus in young (top) and aged (bottom) mice (Scale bar, 100µm). Quantitative comparison of the number of neurons labelled by NeuN in the CA1 region of the hippocampus in young (top) and aged (bottom) mice (n= 6, data are mean ± SEM. *$P<0.05$). (H) Representative examples of the 7 classified criteria to score the strategies mice used to perform in the MWM. Strategies are color coded. (I) Strategy plot reflecting the mean strategy-recruitment values for the first and fourth trials of each day for young (left) and aged (right) mice. Quantification comparison of total block length values of individual mice and their employed strategies over the course of 4-day training period. Grey bars represent control mice and red bars represent VAChT-deficient mice. (n= 8, data are mean ± SEM. *$P<0.05$ **$P<0.01$).

139x74mm (300 x 300 DPI)

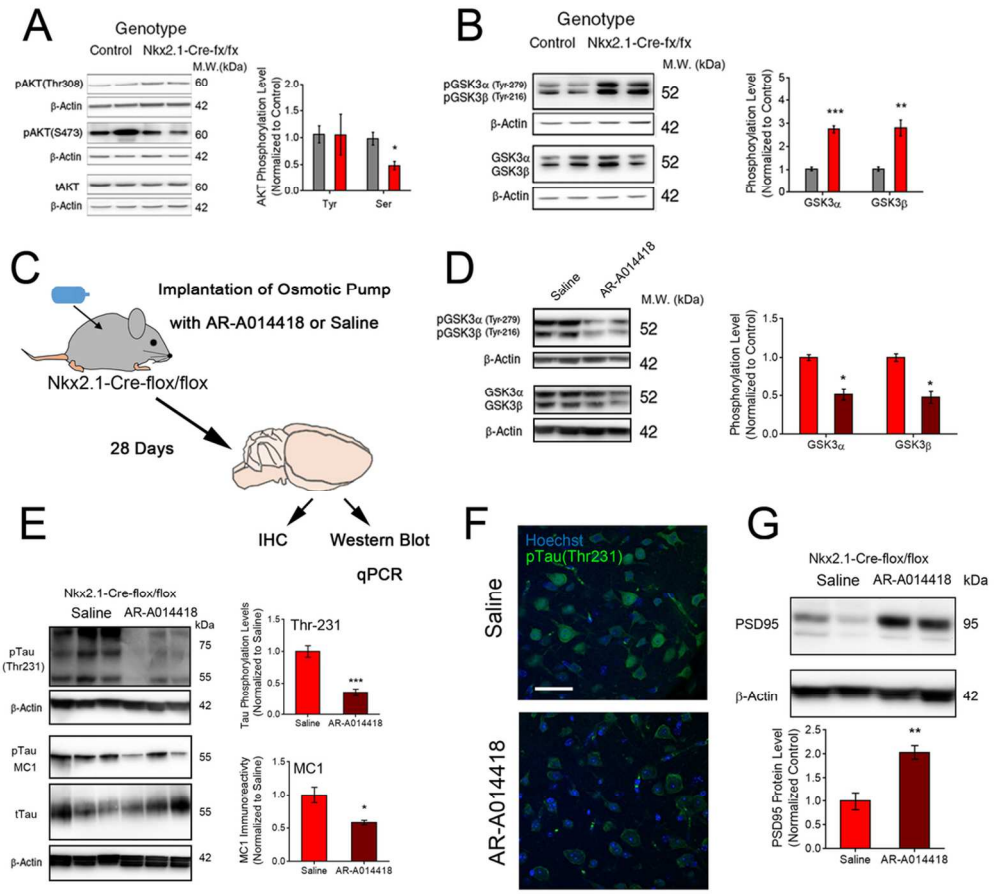

Figure 5. Cholinergic mediated tau hyperphosphorylation is regulated by GSK3 activation. (A) Representative Western-blot and quantification analysis of pAKT(S473) and pAKT(Thr308) levels in the hippocampus of VAChTNkx2.1-Cre-flox/flox mice. (n=4, data are mean ± SEM. *P<0.05 (B) Representative Western blot and quantification analysis of phospho-GSK3α and β in the hippocampus of aged (11-14 month old) controls (left) and VAChTNKx2.1-Cre-flox/flox (right) mice. Levels of pGSK3α and β to the respective GSK3 (n= 5 and 3, data are mean ± SEM. **P<0.01, ***P<0.001). (C) Implantation of osmotic pumps and delivery of AR-A014418 to aged VAChTNKx2.1-Cre-flox/flox mice. (D) Representative Western blot and quantification analysis of phospho-GSK3α and β in the hippocampus of aged VAChTNKx2.1-Cre-flox/flox mice treated with AR-A014418 or saline. (E) Western blot analysis aged VAChTNKx2.1-Cre-flox/flox treated with AR-A014418 or saline for Tau hyper-phosphorylation at T231, MCI immunopositive tau and total Tau protein expression. (F) Representative immunolabelling of reduced T231 Tau in the hippocampus of aged VAChTNKx2.1-Cre-flox/flox mice (Scale bar, 100μm). (G) Western blot analysis for PSD-95 protein levels in the hippocampus of VAChTNkx2.1-Cre-flox/flox mice treated with AR-A014418 or saline. (n= 4 saline treated, n=5 AR-A014418 treated, data are mean ± SEM. *P<0.05 ***P<0.001).
102x93mm (300 x 300 DPI)

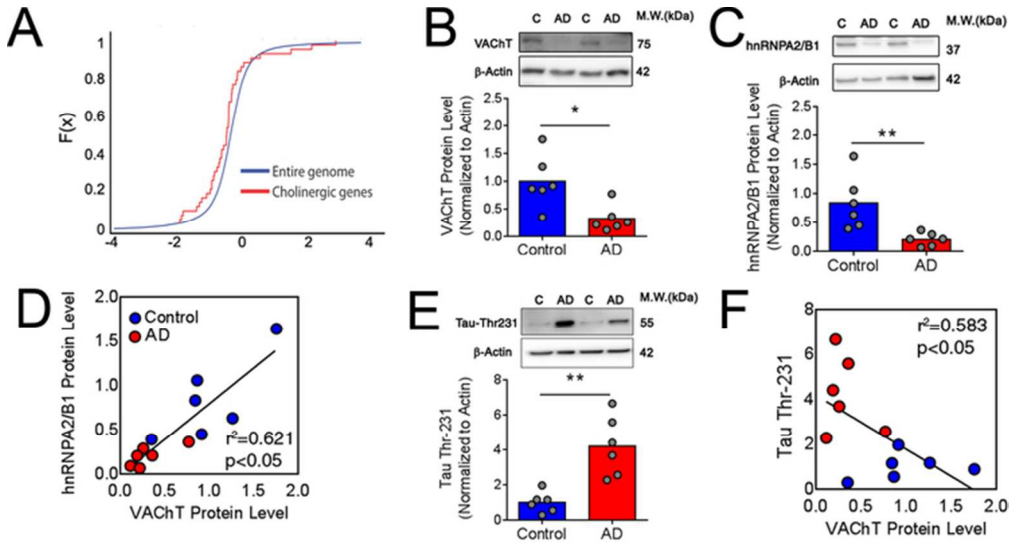

Figure 6. Cholinergic Failure in the human AD Brain associates with loss of hnRNPA2/B1 and hyperphosporylation of tau. (A) Cholinergic Genes are down-regulated in the AD temporal gyrus. Shown are cumulative distribution functions (CDFs) for the global change in the expanded family of cholinergic genes (as listed in Soreq, 2015) compared to global expression patterns between AD and control brain tissues (n= 8, Kolmogorov Smirnov p=0.03, red and blue lines, correspondingly). (B) Western blot analysis of VAChT protein levels in AD brains. (C) Western blot analysis of hnRNPA2/B1 protein levels in AD brains. (D) Correlation between hnRNPA2/B1 protein levels and VAChT protein levels in AD brains. (E) Western blot analysis of Tau-Thr231 phosphorylation levels and (F) correlation between VAChT protein levels and Tau Thr-231 phosphorylation levels. (n= 6, data are mean ± SEM. *P<0.05 **P<0.01).
63x33mm (300 x 300 DPI)

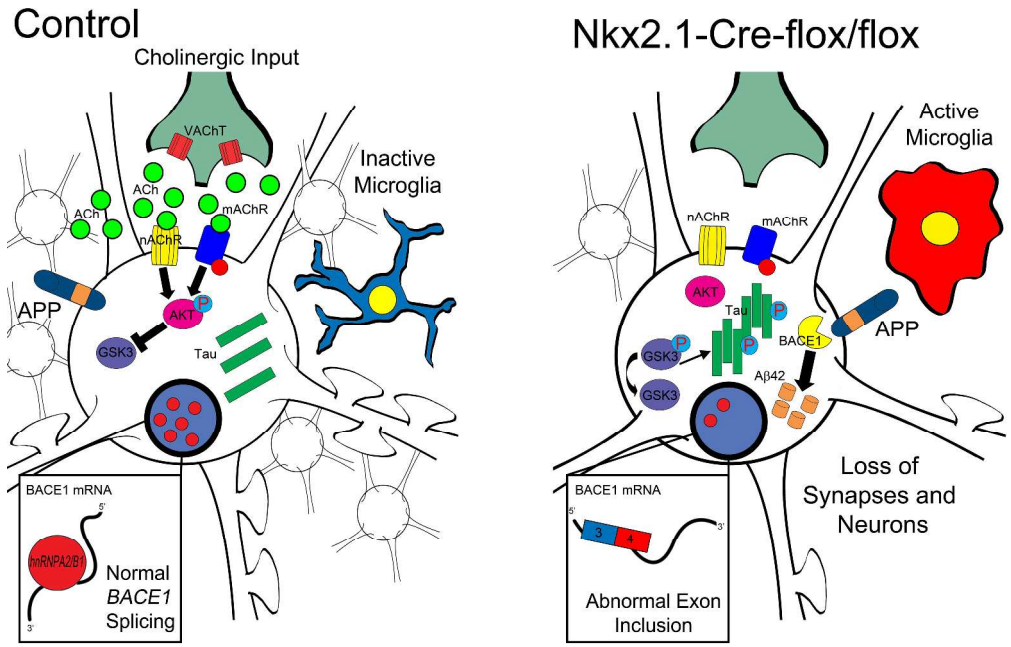

Figure 7. Summary of our findings. (A) In control animals, cholinergic input from the medial septum regulates target neurons in the hippocampus, through nicotinic and muscarinic acetylcholine receptors. Long-term cholinergic signaling maintains transcriptome integrity likely by a combination of muscarinic and nicotinic activation. These maintain balance of signaling pathways that regulate AD-like pathology. (B) Conversely, in cholinergic deficient mice, which models long-term cholinergic dysfunction, lack of signaling by muscarinic and nicotinic receptors affects differential expression of spliceosome-related genes and reductions in hnRNPA2/B1. BACE1 mRNA is abnormally spliced leading to an increase of BACE1 expression. As a consequence, APP processing is altered, yielding accumulation of soluble Aβ peptides. Furthermore, abnormal gene expression influences AKT-GSK3 modulatory genes with consequences for AKT and GSK3 phosphorylation. These changes contribute to increases in pathological tau phosphorylation and misfolding, neuroinflammation, synaptic loss, hippocampal neuronal death and ultimately leading to cognitive decline in these animals.

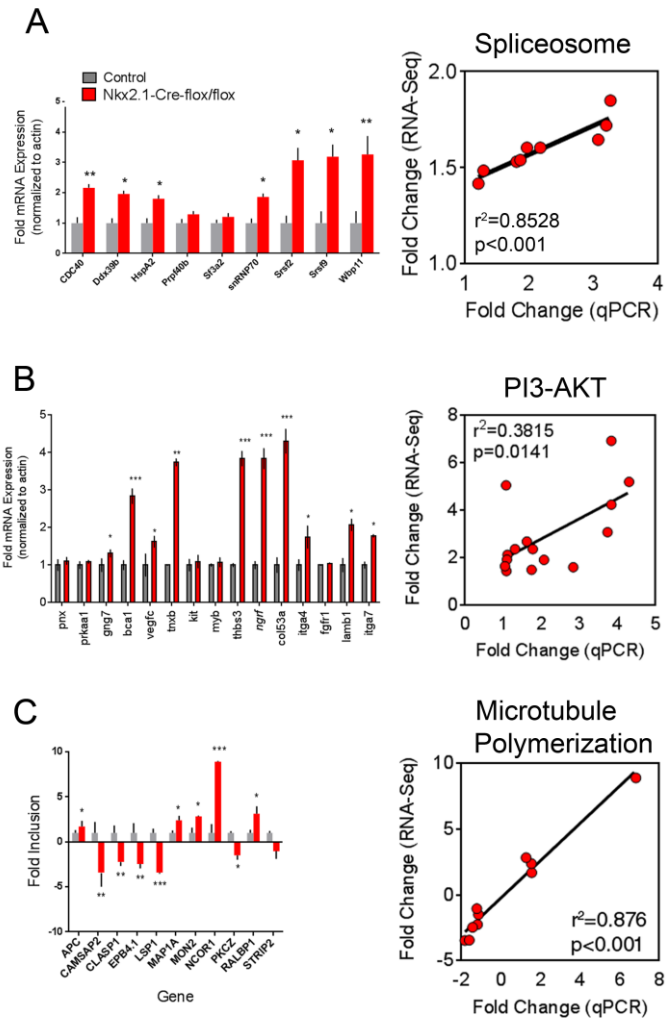

Supplementary Figure 1. qPCR validation of RNA-Seq data. (A) qPCR validation and Pearson's correlation analysis on transcripts annotated to the spliceosome KEGG pathway quantified by RNA-Seq data from the hippocampus of $VAChT^{NKx2.1\text{-}Cre\text{-}flox/flox}$ mice and controls [(r=0.8528, p=0.001), n=6 data are mean ± SEM.]. (B) qPCR validation and Pearson's correlation analysis with RNA-Seq data of transcripts annotated to the PI3k-AKT KEGG pathway [(r=0.8528, p=0.001). (C) qPCR validation and Pearson's correlation analysis of transcripts annotated to the microtubule polymerization pathway [(r=0.8528, p=0.001).

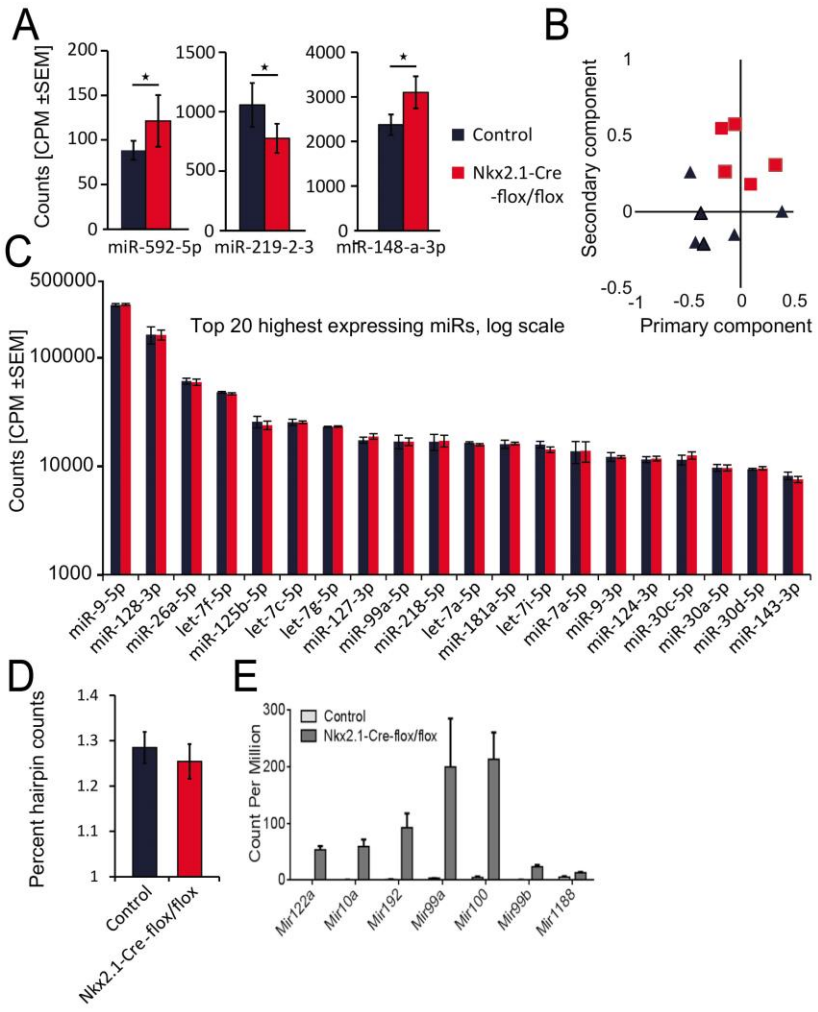

Supplementary Figure 2. Global hippocampal expression of miRNA is not altered in VAChT deficient mice. (A) Small RNA sequencing from six VAChT$^{Nkx2.1\text{-}Cre\text{-}flox/flox}$ mice and five controls demonstrated miR-592-5p, miR-219-2-3 and 148a-3p as differentially expressed (DE) after FDR correction ($P<0.05$). (B) Principal Component Analysis (PCA) showed marginal separation of the two groups, suggesting that VAChT transcript removal does not induce a global change in small RNA expression. (C) Extent of absolute change was limited, as none of the top 20 miRNAs expressed in the hippocampus were modified, leaving 82% of hippocampal miRNAs unchanged. (D) Similar fractions of small RNA reads mapped to parts of the pre-miRNA molecules other than the mature-miRNA in VAChT$^{Nkx2.1\text{-}Cre\text{-}flox/flox}$ mice and controls (E) Processing rate and/or efficacy might be affected, as a set of 7 seemingly unmodified miRNAs presented drastically reduced pre-miRNA levels when quantified by long RNA sequencing in VAChT$^{Nkx2.1\text{-}Cre\text{-}flox/flox}$ mice.

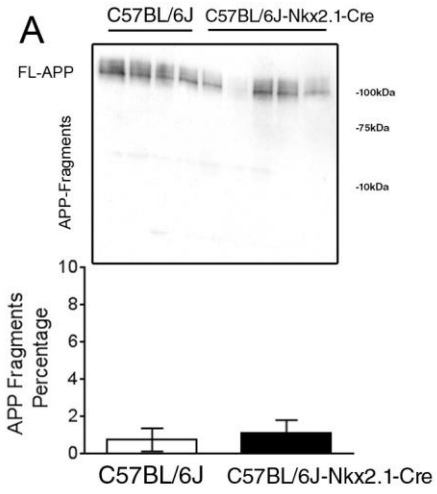

Supplementary Figure 3. Absence of altered APP processing in aged (11-14 month old) C57/BJ6-Nkx2.1-Cre mice (A) Western blot of APP processing from Tris-soluble fraction and quantification of APP fragments detected in aged C57BL/6J-Nkx2.1-Cre mice (11-14 month old) showing no significant differences compared to controls (n=4).(Data are mean +/- S.E.M.).

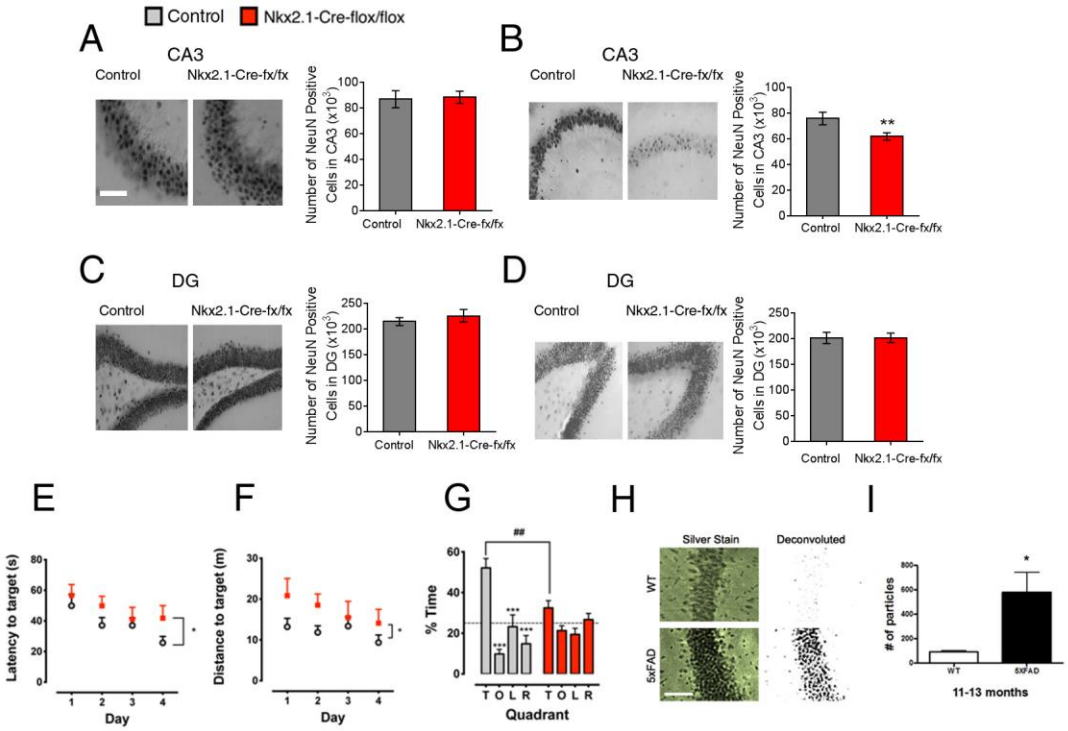

Supplementary Figure 4. Estimation of neuronal volume in the CA3 and DG region of the hippocampus of young (3-6) and aged (11-14) month old cholinergic deficient mice as well as cognitive deficits in aged cholinergic deficient mice. (A) Young VAChT$^{Nkx2.1\text{-}Cre\text{-}flox/flox}$ mice show no change in number of NeuN positive cells in the CA3 ($t_{(18)}$=0.1894, p=0.8519), However in (B) there is a significant reduction in number of NeuN positive cells in the CA3 of aged VAChT$^{Nkx2.1\text{-}Cre\text{-}flox/flox}$ mice ($t_{(18)}$=2.454, p=0.0246). No change in the number of NeuN positive cells in the DG region was observed in either young (C) ($t_{(18)}$=0.7814, p=0.4447) or old (D) ($t_{(18)}$=0.01758, p=0.9862) VAChT$^{Nkx2.1\text{-}Cre\text{-}flox/flox}$ mice (Data are mean +/- S.E.M., **p<0.01, n=9). Significantly impaired latency (E) (RM-ANOVA, main effect of genotype $F_{(1,7)}$=6.359, p=0.0397), and distance to reach the platform (F) (RM-ANOVA, main effect of genotype $F_{(1,7)}$=7.845, p=0.0265) in aged (11-14 month old) VAChT$^{Nkx2.1\text{-}Cre\text{-}flox/flox}$ mice. (G) Aged (11-14 month old) VAChT$^{Nkx2.1\text{-}Cre\text{-}flox/flox}$ mice do not show a preference for the target platform during the probe trial portion of the MWM task (RM-ANOVA, main effect of interaction $F_{(3,21)}$=6.068, p<0.0038). (Data are mean +/- S.E.M., *p<0.05, **p<0.01, ***p<0.001, n=8). (H) Representative images of silver staining procedure from 11-14 month old wild-type and 5xFAD mice. (I) Quantification of percent silver stain area from 11-14 month old wild-type and 5xFAD mice (Data are mean +/- S.E.M., ***p<0.001, n=3). Scale bar 100 µm.

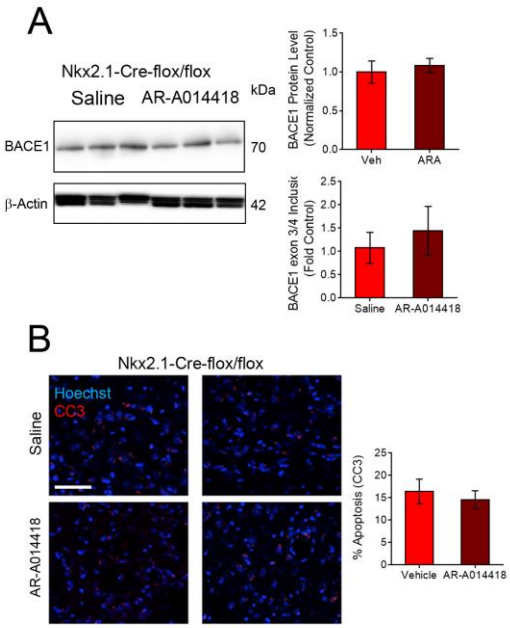

Supplementary Figure 5. **Cholinergic mediated age dependent pathology is partially mediated by GSK3 hyper-phosphorylation.** (A) Representative Western blot and quantification analysis of BACE1 protein levels, along with qPCR analysis of alternative splicing of exon 3/4 of the BACE1 gene in hippocampus of VAChT$^{NKx2.1\text{-}Cre\text{-}flox/flox}$ treated with AR-A014418 or saline. (B) Quantification of activated caspase-3 immunolabelling in the hippocampus of VAChT$^{Nkx2.1\text{-}Cre\text{-}flox/flox}$ mice treated with AR-A014418 or saline (Scale bar, 100μm) (n= 4 saline treated, n=5 AR-A014418 treated, data are mean ± SEM. *P<0.05 **P<0.01).

Supplementary Table 1. Genes in either the AKT pathway (grey shading), Spliceosome pathway (blue shading), or Regulation of Microtubule Polymerization (green shading) and role(s) in AD-like pathology.

Gene	Link to AD
Bcar1	Linked to APP transcription (1).
Col5a3	SNP linked to AD (2).
Fgfr1	Altered expression in aging (3).
Gng7	Associated with depression in the elderly (4).
Itga4	Protein alterations in animal model of neurodegeneration (5). Upregulated in astrocytes in AD brain (6). Potential to bind Ab (7).
Itga7	Potential to bind Ab (7).
Kit	Mediates cell survival and apoptosis via AKT (8)
Lamb1	SNP linked to AD (9)
Myb	Regulates neuronal apoptosis (10)
Ngfr	Up-regulated in AD brain (11) SNP linked to AD (12)
Pck2	SNP linked to AD (9) Altered transcription in AD brain (13)
Prkaa1	SNP linked to AD (14)
Prlr	Up-regulated in rat model of AD (15)
Pxn	Up-regulated in AD brain (16)
Thbs3	Altered transcription in AD brain (17)
Tnxb	SNP linked to AD (18, 19)
Vegfc	Increased levels in CSF of AD patients (20)
Cdc40	Linked to alternative splicing in neurodegeneration (21)
Ddx39b	SNP linked to Late-Onset-AD (22)
Hspa2	SNP linked to Late-Onset-AD (23, 24)
Prpf40b	Implicated in human neurodegeneration (25)
Sf3a2	Altered in aging mouse brain(26)
Snrnp70	Up-regulated and aggregated in AD brain (27)
Srsf2	Regulates splicing events in AD (28)
Srsf9	Regulates splicing events in AD (29)
Wbp11	Upregulated in accelerated aging murine model (30)

APC	Increased expression in AD brain (31)
CAMSAP2	Altered protein levels in animal model of neurodegeneration (32)
CLASP1	No known link to AD
EBP4.1	Interacts with APP protein in vivo (33)
LSP1	Epigenetic modifications in AD mouse model (34)
MAP1A	Upregulated in tau deficient mice (35) Binds soluble Aβ *in vitro (36)*
MON2	No known link to AD
NCOR1	Protein expression altered by Aβ and tau (37)
PKCZ	Altered activity in AD brain (38)
RALBP1	Transcription altered in AD brain (39)
STRIP2	Decreased expression in neurodegeneration (40)

1. Seenundun S, and Robaire B. Time-dependent rescue of gene expression by androgens in the mouse proximal caput epididymidis-1 cell line after androgen withdrawal. *Endocrinology.* 2007;148(1):173-88.
2. Silver M, Janousova E, Hua X, Thompson PM, and Montana G. Identification of gene pathways implicated in Alzheimer's disease using longitudinal imaging phenotypes with sparse regression. *NeuroImage.* 2012;63(3):1681-94.
3. Walker DG, Terai K, Matsuo A, Beach TG, McGeer EG, and McGeer PL. Immunohistochemical analyses of fibroblast growth factor receptor-1 in the human substantia nigra. Comparison between normal and Parkinson's disease cases. *Brain research.* 1998;794(2):181-7.
4. Schol-Gelok S, Janssens AC, Tiemeier H, Liu F, Lopez-Leon S, Zorkoltseva IV, Axenovich TI, van Swieten JC, Uitterlinden AG, Hofman A, et al. A genome-wide screen for depression in two independent Dutch populations. *Biological psychiatry.* 2010;68(2):187-96.
5. Karlsson O, Berg AL, Lindstrom AK, Hanrieder J, Arnerup G, Roman E, Bergquist J, Lindquist NG, Brittebo EB, and Andersson M. Neonatal exposure to the cyanobacterial toxin BMAA induces changes in protein expression and neurodegeneration in adult hippocampus. *Toxicological sciences : an official journal of the Society of Toxicology.* 2012;130(2):391-404.
6. Orre M, Kamphuis W, Osborn LM, Jansen AH, Kooijman L, Bossers K, and Hol EM. Isolation of glia from Alzheimer's mice reveals inflammation and dysfunction. *Neurobiology of aging.* 2014;35(12):2746-60.
7. Sabo S, Lambert MP, Kessey K, Wade W, Krafft G, and Klein WL. Interaction of beta-amyloid peptides with integrins in a human nerve cell line. *Neuroscience letters.* 1995;184(1):25-8.
8. Blume-Jensen P, Janknecht R, and Hunter T. The kit receptor promotes cell survival via activation of PI 3-kinase and subsequent Akt-mediated phosphorylation of Bad on Ser136. *Current biology : CB.* 1998;8(13):779-82.
9. Taguchi K, Yamagata HD, Zhong W, Kamino K, Akatsu H, Hata R, Yamamoto T, Kosaka K, Takeda M, Kondo I, et al. Identification of hippocampus-related candidate genes for Alzheimer's disease. *Annals of neurology.* 2005;57(4):585-8.
10. Liu DX, Biswas SC, and Greene LA. B-myb and C-myb play required roles in neuronal apoptosis evoked by nerve growth factor deprivation and DNA damage. *The Journal of neuroscience : the official journal of the Society for Neuroscience.* 2004;24(40):8720-5.

11. Scott SA, Mufson EJ, Weingartner JA, Skau KA, and Crutcher KA. Nerve growth factor in Alzheimer's disease: increased levels throughout the brain coupled with declines in nucleus basalis. *The Journal of neuroscience : the official journal of the Society for Neuroscience.* 1995;15(9):6213-21.
12. Cozza A, Melissari E, Iacopetti P, Mariotti V, Tedde A, Nacmias B, Conte A, Sorbi S, and Pellegrini S. SNPs in neurotrophin system genes and Alzheimer's disease in an Italian population. *Journal of Alzheimer's disease : JAD.* 2008;15(1):61-70.
13. Brooks WM, Lynch PJ, Ingle CC, Hatton A, Emson PC, Faull RL, and Starkey MP. Gene expression profiles of metabolic enzyme transcripts in Alzheimer's disease. *Brain research.* 2007;1127(1):127-35.
14. Clarimon J, Djaldetti R, Lleo A, Guerreiro RJ, Molinuevo JL, Paisan-Ruiz C, Gomez-Isla T, Blesa R, Singleton A, and Hardy J. Whole genome analysis in a consanguineous family with early onset Alzheimer's disease. *Neurobiology of aging.* 2009;30(12):1986-91.
15. Bakalash S, Pham M, Koronyo Y, Salumbides BC, Kramerov A, Seidenberg H, Berel D, Black KL, and Koronyo-Hamaoui M. Egr1 expression is induced following glatiramer acetate immunotherapy in rodent models of glaucoma and Alzheimer's disease. *Investigative ophthalmology & visual science.* 2011;52(12):9033-46.
16. Liang D, Han G, Feng X, Sun J, Duan Y, and Lei H. Concerted perturbation observed in a hub network in Alzheimer's disease. *PloS one.* 2012;7(7):e40498.
17. Kalback W, Esh C, Castano EM, Rahman A, Kokjohn T, Luehrs DC, Sue L, Cisneros R, Gerber F, Richardson C, et al. Atherosclerosis, vascular amyloidosis and brain hypoperfusion in the pathogenesis of sporadic Alzheimer's disease. *Neurological research.* 2004;26(5):525-39.
18. Meda SA, Narayanan B, Liu J, Perrone-Bizzozero NI, Stevens MC, Calhoun VD, Glahn DC, Shen L, Risacher SL, Saykin AJ, et al. A large scale multivariate parallel ICA method reveals novel imaging-genetic relationships for Alzheimer's disease in the ADNI cohort. *NeuroImage.* 2012;60(3):1608-21.
19. Sherva R, Baldwin CT, Inzelberg R, Vardarajan B, Cupples LA, Lunetta K, Bowirrat A, Naj A, Pericak-Vance M, Friedland RP, et al. Identification of novel candidate genes for Alzheimer's disease by autozygosity mapping using genome wide SNP data. *Journal of Alzheimer's disease : JAD.* 2011;23(2):349-59.
20. Tarkowski E, Issa R, Sjogren M, Wallin A, Blennow K, Tarkowski A, and Kumar P. Increased intrathecal levels of the angiogenic factors VEGF and TGF-beta in Alzheimer's disease and vascular dementia. *Neurobiology of aging.* 2002;23(2):237-43.
21. Tollervey JR, Wang Z, Hortobagyi T, Witten JT, Zarnack K, Kayikci M, Clark TA, Schweitzer AC, Rot G, Curk T, et al. Analysis of alternative splicing associated with aging and neurodegeneration in the human brain. *Genome research.* 2011;21(10):1572-82.
22. Mohsen S, Hadi B, Kourosh K, Kioomars S, Mehdi B, and Khorshid Hamid Reza K. Association Study of IL-4 -590 C/T and DDX39B -22 G/C Polymorphisms with The Risk of Late-Onset Alzheimer's Disease in Iranian Population. *Current aging science.* 2015.
23. Clarimon J, Bertranpetit J, Boada M, Tarraga L, and Comas D. HSP70-2 (HSPA1B) is associated with noncognitive symptoms in late-onset Alzheimer's disease. *Journal of geriatric psychiatry and neurology.* 2003;16(3):146-50.
24. Broer L, Ikram MA, Schuur M, DeStefano AL, Bis JC, Liu F, Rivadeneira F, Uitterlinden AG, Beiser AS, Longstreth WT, et al. Association of HSP70 and its co-chaperones with Alzheimer's disease. *Journal of Alzheimer's disease : JAD.* 2011;25(1):93-102.
25. Passani LA, Bedford MT, Faber PW, McGinnis KM, Sharp AH, Gusella JF, Vonsattel JP, and MacDonald ME. Huntingtin's WW domain partners in Huntington's disease post-mortem brain

fulfill genetic criteria for direct involvement in Huntington's disease pathogenesis. *Human molecular genetics.* 2000;9(14):2175-82.

26. Meshorer E, and Soreq H. Pre-mRNA splicing modulations in senescence. *Aging cell.* 2002;1(1):10-6.
27. Bai B, Hales CM, Chen PC, Gozal Y, Dammer EB, Fritz JJ, Wang X, Xia Q, Duong DM, Street C, et al. U1 small nuclear ribonucleoprotein complex and RNA splicing alterations in Alzheimer's disease. *Proceedings of the National Academy of Sciences of the United States of America.* 2013;110(41):16562-7.
28. Raj T, Ryan KJ, Replogle JM, Chibnik LB, Rosenkrantz L, Tang A, Rothamel K, Stranger BE, Bennett DA, Evans DA, et al. CD33: increased inclusion of exon 2 implicates the Ig V-set domain in Alzheimer's disease susceptibility. *Human molecular genetics.* 2014;23(10):2729-36.
29. Qian W, and Liu F. Regulation of alternative splicing of tau exon 10. *Neuroscience bulletin.* 2014;30(2):367-77.
30. Carter TA, Greenhall JA, Yoshida S, Fuchs S, Helton R, Swaroop A, Lockhart DJ, and Barlow C. Mechanisms of aging in senescence-accelerated mice. *Genome biology.* 2005;6(6):R48.
31. Leroy K, Duyckaerts C, Bovekamp L, Muller O, Anderton BH, and Brion JP. Increase of adenomatous polyposis coli immunoreactivity is a marker of reactive astrocytes in Alzheimer's disease and in other pathological conditions. *Acta neuropathologica.* 2001;102(1):1-10.
32. McGorum BC, Pirie RS, Eaton SL, Keen JA, Cumyn EM, Arnott DM, Chen W, Lamont DJ, Graham LC, Llavero Hurtado M, et al. Proteomic Profiling of Cranial (Superior) Cervical Ganglia Reveals Beta-Amyloid & Ubiquitin Proteasome System Perturbations in an Equine Multiple System Neuropathy. *Molecular & cellular proteomics : MCP.* 2015.
33. Bai Y, Markham K, Chen F, Weerasekera R, Watts J, Horne P, Wakutani Y, Bagshaw R, Mathews PM, Fraser PE, et al. The in vivo brain interactome of the amyloid precursor protein. *Molecular & cellular proteomics : MCP.* 2008;7(1):15-34.
34. Cong L, Jia J, Qin W, Ren Y, and Sun Y. Genome-wide analysis of DNA methylation in an APP/PS1 mouse model of Alzheimer's disease. *Acta neurologica Belgica.* 2014;114(3):195-206.
35. Ma QL, Zuo X, Yang F, Ubeda OJ, Gant DJ, Alaverdyan M, Kiosea NC, Nazari S, Chen PP, Nothias F, et al. Loss of MAP function leads to hippocampal synapse loss and deficits in the Morris Water Maze with aging. *The Journal of neuroscience : the official journal of the Society for Neuroscience.* 2014;34(21):7124-36.
36. Clemmensen C, Aznar S, Knudsen GM, and Klein AB. The microtubule-associated protein 1A (MAP1A) is an early molecular target of soluble Abeta-peptide. *Cellular and molecular neurobiology.* 2012;32(4):561-6.
37. Hoerndli FJ, Pelech S, Papassotiropoulos A, and Gotz J. Abeta treatment and P301L tau expression in an Alzheimer's disease tissue culture model act synergistically to promote aberrant cell cycle re-entry. *The European journal of neuroscience.* 2007;26(1):60-72.
38. Moore P, White J, Christiansen V, and Grammas P. Protein kinase C-zeta activity but not level is decreased in Alzheimer's disease microvessels. *Neuroscience letters.* 1998;254(1):29-32.
39. Zhang L, Guo XQ, Chu JF, Zhang X, Yan ZR, and Li YZ. Potential hippocampal genes and pathways involved in Alzheimer's disease: a bioinformatic analysis. *Genetics and molecular research : GMR.* 2015;14(2):7218-32.
40. Desplats PA, Kass KE, Gilmartin T, Stanwood GD, Woodward EL, Head SR, Sutcliffe JG, and Thomas EA. Selective deficits in the expression of striatal-enriched mRNAs in Huntington's disease. *Journal of neurochemistry.* 2006;96(3):743-57.

Supplementary Table 2: Data for cohort of human brain samples, collected from the Netherland Brain Bank, from which total RNA was extracted and sequenced, n=24.

NBB id	sex	age	Post mortem delay	ph	weight	region
2008-047	M	77	06:35	6.10	1250	superior temporalis gyrus
2000-066	M	80	04:20	7.08	1160	inferior temporalis gyrus
2007-025	M	82	05:15	6.34	1182	superior temporalis gyrus
2007-052	M	82	04:15	6.41	1205	medial temporalis gyrus
2009-040	M	83	06:10	5.91	1102	superior temporalis gyrus
2008-029	M	84	08:05	5.95	1195	superior temporalis gyrus
2001-044	M	85	04:25	6.20	1383	superior temporalis gyrus
2001-063	M	85	04:45	6.38	1215	superior temporalis gyrus
2010-016	M	86	06:15	?	1211	superior temporalis gyrus
2009-107	M	88	04:40	6.22	1054	superior temporalis gyrus
2005-010	M	93	04:30	6.46	1040	superior temporalis gyrus
2002-087	M	71	07:40	6.20	1150	superior temporalis gyrus
2001-016	M	77	08:25	7.19	1118	superior temporalis gyrus
2000-015	M	78	05:35	6.63	1417	inferior temporalis gyrus
2005-044	M	80	07:15	5.80	1331	superior temporalis gyrus
2001-021	M	82	07:40	6.07	1318	inferior temporalis gyrus
2009-005	M	82	05:10	6.75	1087	superior temporalis gyrus
2001-086	M	88	07:00	6.84	1368	superior temporalis gyrus
2003-035	M	96	06:30	6.65	1300	superior temporalis gyrus
2005-019	M	74	05:00	6.70	1115	superior temporalis gyrus
2003-084	M	82	10:00	6.53	1488	superior temporalis gyrus
2009-039	M	82	12:55	6.21	1406	superior temporalis gyrus
2005-073	M	87	06:05	6.96	1468	superior temporalis gyrus
2009-075	M	88	07:00	6.76	1230	superior temporalis gyrus

Supplementary Table 3: Number of detected genes (RPKM>1) per patient, per SQUARE field. Rows are patients and columns are SQUARE fields.

		1	2	3	4	5	6	7	8	9	10	11	12
AD	1	6152	6729	6154	7224	9942	6284	4273	5176	6504	7879	5815	7500
	2	6961	6995	6251	7516	9611	6478	4549	5294	6698	7778	6204	7747
	3	6945	7107	6627	7388	9746	6221	4529	5037	6789	7983	6145	6059
	4	6811	6704	6530	7555	9664	6193	2877	4868	6250	7976	6246	8079
	5	6123	6417	5848	7628	9529	5953	4637	4639	6140	7481	5814	7654
	6	6956	7093	6308	7469	9927	6730	4542	4951	6091	7465	5699	6550
	7	6310	6217	5749	7176	9410	5910	4393	4695	6247	7203	5531	7122
	8	6770	6999	6436	7352	9675	6730	4451	5233	6761	7500	6114	7589
Con	9	6374	6456	5957	6785	9250	6039	3889	4726	6506	7182	5307	6633
	10	6820	6919	6083	6883	9270	5950	4367	4861	6763	7729	5266	6545
	11	5771	6029	5191	6705	9445	5654	4197	4565	6188	6804	5649	6986
	12	5660	7181	6486	7208	10160	7867	5148	5422	6939	8082	6243	6555
	13	6332	6962	6220	6468	9430	6576	3876	5126	6959	7805	5361	6657
	14	6103	6486	5507	7139	9583	5781	4467	4604	6150	7328	5632	7412
	15	6380	6414	5592	6486	9377	5557	3940	4277	6225	7869	5571	7090
	16	6511	6673	6217	7495	9710	6147	4238	4947	6788	8011	5732	7296
	17	6265	6450	5903	7247	9142	5907	4403	4718	6022	7212	5424	7478
	18	7153	7552	6945	7596	9822	6549	4382	5424	7282	8388	5926	7285
	19	6294	5943	5668	7300	9259	5648	4255	4416	6108	7468	5690	7321
	20	6268	6583	5753	7391	9732	6125	4635	4815	5896	7847	5733	7395
	21	7674	7822	6969	8201	10588	7826	5027	5787	7348	8095	6059	7434
	22	7274	7185	6793	7824	9945	6982	4755	5377	7258	8310	6185	7737
	23	7149	7073	6654	7206	9895	6774	4890	5274	6915	8485	5796	8190

24	5676	6113	5303	6938	9863	6393	4630	4835	6651	7721	5964	6474